

1 **Calcium-independent but voltage-dependent secretion (CivDS) mediates**
2 **synaptic transmission in a mammalian central synapse**

3
4 Yuan Wang^{1, †}, Rong Huang^{1, †}, Zuying Chai^{1, †}, Changhe Wang^{6, †}, Xingyu
5 Du^{1,2}, Yuqi Hang^{1,2}, Yongxin Xu¹, Jie Li¹, Xiaohan Jiang¹, Xi Wu^{1,2},
6 Zhongjun Qiao¹, Yinglin Li¹, Bing Liu¹, Xianying Zhang⁵, Peng Cao⁵,
7 Feipeng Zhu¹ and Zhuan Zhou^{1-4, *}

8
9 ¹State Key Laboratory of Membrane Biology, Institute of Molecular Medicine,
10 Peking University, Beijing 100871, China; ²Peking-Tsinghua Center for Life
11 Sciences, Beijing 100871, China; ³PKU-IDG/McGovern Institute for Brain Research,
12 Beijing 100871, China; ⁴Beijing Key Laboratory of Cardiometabolic Molecular
13 Medicine, Beijing 100871, China; ⁵National Institute of Biological Sciences, Beijing
14 102206, China; ⁶School of Life Science and Technology, Xi'an Jiaotong University,
15 Xi'an 710049, China.

16
17 †Equal contributors

18 *For correspondence: zzhou@pku.edu.cn

19 Competing interests: The authors declare no competing interests.

20
21 **Address for editorial correspondence and proof:**

22 Dr. Zhuan Zhou
23 Institute of Molecular Medicine,
24 Peking University
25 5 Yiheyuan Road,
26 Beijing 100871, China
27 Tel & Fax: ++86-10-6275-3212
28 Email: zzhou@pku.edu.cn

29

30

31 **Abstract**

32 A central principle of synaptic transmission is that action potential-induced
33 presynaptic neurotransmitter release occurs exclusively *via* Ca²⁺-dependent secretion
34 (CDS). The discovery and mechanistic investigations of Ca²⁺-independent but
35 voltage-dependent secretion (CiVDS) have demonstrated that the action potential *per*
36 *se* is sufficient to trigger neurotransmission in the somata of primary sensory and
37 sympathetic neurons in mammals. One key question remains, however, whether
38 CiVDS contributes to central synaptic transmission. Here we report, in the central
39 transmission from presynaptic (dorsal root ganglion) to postsynaptic (spinal dorsal
40 horn) neurons, (1) excitatory postsynaptic currents (EPSCs) are mediated by
41 glutamate transmission through both CiVDS (up to 87%) and CDS; (2)
42 CiVDS-EPSCs are independent of extracellular and intracellular Ca²⁺; (3) CiVDS
43 is >100 times faster than CDS in vesicle recycling with much less short-term
44 depression; (4) the fusion machinery of CiVDS includes Cav2.2 (voltage sensor) and
45 SNARE (fusion pore). Together, an essential component of activity-induced EPSCs is
46 mediated by CiVDS in a central synapse.

47

48 **Keywords:** Ca²⁺-dependent secretion, Ca²⁺-independent but voltage-dependent
49 secretion (CiVDS), synaptic transmission, dorsal root ganglion, dorsal horn,
50 excitatory postsynaptic currents, Cav2.2, SNARE

51

52 **Introduction**

53 The tight coupling of synaptic neurotransmitter release to the action potential within a
54 millisecond is critical for neuronal communication and brain function (Augustine,
55 Charlton, & Smith, 1987; Hopfield, 1995; Neher & Sakaba, 2008; Sabatini & Regehr,
56 1996). The classical view of synaptic transmission is based on the “Ca²⁺ hypothesis”:
57 presynaptic membrane depolarization opens voltage-gated Ca²⁺ channels (VGCCs),
58 which leads to Ca²⁺ influx into the cytosol and triggers vesicular neurotransmitter
59 release (Augustine et al., 1987; Geppert et al., 1994; Jackson & Chapman, 2006; Katz
60 & Miledi, 1967; Neher & Sakaba, 2008; Sudhof, 2012). In this half-century dogma,
61 synaptic transmission is directly triggered by Ca²⁺, synaptotagmin, and SNARE
62 complex assembly (Jahn & Scheller, 2006; Sollner et al., 1993), or membrane
63 depolarization triggers synaptic transmission indirectly by mediating Ca²⁺ influx
64 through VGCCs (Felmy, Neher, & Schneggenburger, 2003; Jackson & Chapman,
65 2006; Meinrenken, Borst, & Sakmann, 2003; Nanou & Catterall, 2018; Neher &
66 Zucker, 1993; Parnas & Parnas, 2010). Since 2002, this Ca²⁺ hypothesis has
67 encountered exceptions in a series of reports on Ca²⁺-independent but
68 voltage-dependent secretion (CiVDS) in primary sensory dorsal root ganglion (DRG)
69 neurons (Chai et al., 2017; Huang et al., 2019; C. Zhang et al., 2004; C. Zhang &
70 Zhou, 2002; Zheng et al., 2009), where action potentials *per se* directly trigger
71 somatic vesicular exocytosis.

72 In addition to the DRG (C. Zhang & Zhou, 2002), somatic CiVDS has been
73 extended to trigeminal ganglion neurons (Sforna, Franciolini, & Catacuzzeno, 2019),

74 sympathetic superior cervical ganglion neurons, and neuroendocrine chromaffin cells
75 (Huang et al., 2019; Moya-Diaz et al., 2019). Further studies have revealed unique
76 features of CiVDS compared with Ca²⁺-dependent secretion (CDS): (1) rather than
77 slow and dynamin-dependent endocytosis following CDS (Artalejo, Elhamdani, &
78 Palfrey, 2002; Ferguson et al., 2007; Wu et al., 2019), CiVDS is coupled to a fast and
79 dynamin-independent but protein kinase A-dependent endocytosis (C. Zhang et al.,
80 2004); (2) the vesicle pool replenishment of CiVDS is much faster than that of CDS
81 (Huang et al., 2019; C. Zhang & Zhou, 2002); (3) at the single-vesicle level, CiVDS
82 has a smaller quantal size and faster release kinetics (Huang et al., 2019); and (4)
83 VGCC activation plays dual roles --- indirectly triggering CDS *via* Ca²⁺-influx, and
84 directly triggering CiVDS through the “synprint” binding domain between VGCC and
85 SNARE (Chai et al., 2017; Huang et al., 2019; Nanou & Catterall, 2018). This enables
86 a faster on/off-gating for vesicle fusion *via* CiVDS in somata (Chai et al., 2017;
87 Huang et al., 2019; Liu et al., 2011). The key question remains, however, whether
88 CiVDS occurs in synaptic transmission.

89 In the present study, by combining electrophysiological recordings, live-cell
90 pHluorin imaging, optogenetic stimulation, and genetic manipulations, we report that
91 CiVDS is present in the central synapses between presynaptic DRG and postsynaptic
92 spinal dorsal horn (DH) neurons. The CiVDS-EPSC has much less short-term
93 depression than that of CDS-EPSC, and predominates during sustained neuronal
94 activity. Altogether, this work provides the first example of CiVDS-mediated synaptic
95 transmission and demonstrates complementary roles of CiVDS and CDS under

96 physiological conditions.

97

98 **Results**

99 **CiVDS mediates synaptic transmission in co-cultured DRG and DH neurons**

100 Our previous reports have shown robust CiVDS in the somata of freshly-isolated
101 DRG neurons (Chai et al., 2017; C. Zhang et al., 2004; C. Zhang & Zhou, 2002;
102 Zheng et al., 2009). To investigate whether CiVDS functions in synapses, we
103 co-cultured DRG neurons with postsynaptic DH neurons in which excitatory
104 postsynaptic currents (EPSCs) were collected with whole-cell patch-clamp recordings
105 (**Figure 1A**). Strikingly, local pulses of electrical field stimulation evoked EPSCs in
106 postsynaptic DH neurons, even in 1 mM EGTA (a potent Ca^{2+} chelator)-containing
107 Ca^{2+} -free (0Ca) bath solution (**Figure 1A**). Intracellular Ca^{2+} ($[\text{Ca}^{2+}]_i$) recording
108 validated that there was indeed no $[\text{Ca}^{2+}]_i$ rise during recordings in the 0Ca solution
109 (**Figures 1A, Figure1-figure supplement 1**). The amplitude of EPSCs in 0Ca solution
110 was ~50% of that in the standard 2 mM Ca^{2+} (2Ca) solution (**Figure 1D**). In contrast,
111 the EPSCs recorded in cultured hippocampal neurons were fully dependent on
112 extracellular Ca^{2+} (**Figure 1B**), indicating the absence of CiVDS during synaptic
113 transmission in hippocampal neurons and confirming that the 1 mM EGTA-containing
114 Ca^{2+} -free solution was sufficient to block Ca^{2+} transient at synapses.

115 To further exclude the possible contribution of intracellular microdomain Ca^{2+} ,
116 BAPTA-AM, a potent Ca^{2+} chelator, were pre-loaded into the co-cultured neurons.
117 Consistent with our previous reports on somatic secretion (Chai et al., 2017; Huang et

118 al., 2019; C. Zhang & Zhou, 2002), BAPTA had no effect on the EPSCs recorded in
119 the 0Ca solution, but reduced the EPSCs recorded in 2Ca to that in 0Ca (**Figure**
120 **1C-D**). Thus, under physiological conditions (2Ca), the evoked EPSC contains both a
121 CiVDS-mediated EPSC (CiVDS-EPSC), and a pure CDS-mediated EPSC
122 (CDS-EPSC), or EPSC (2Ca) = CiVDS-EPSC + CDS-EPSC.

123 We next assessed the vesicle recycling rate by using paired-pulse stimuli with
124 different time intervals. Consistent with our previous findings in somatic secretion (C.
125 Zhang & Zhou, 2002), the 80% recovery of the total (CiVDS + CDS) EPSC recorded
126 in 2Ca solution required >5 s intervals (**Figure 1E-F**). In contrast, 80% recovery of
127 the CiVDS-EPSC was achieved within 50 ms (**Figure 1E**), indicating a >100 times
128 faster recycling rate/replenishment of vesicle pools in CiVDS than that in CDS in
129 DRG synaptic terminals. In addition, we used physiological 10-Hz train stimulation to
130 evaluate the contribution of CiVDS during sustained synaptic transmission (Fang,
131 McMullan, Lawson, & Djouhri, 2005; Xu, Huang, & Zhao, 2000; Zheng et al., 2009).
132 Intriguingly, CiVDS-EPSCs showed much less short-term depression than the total
133 EPSCs in 2Ca solution (**Figure 1G-H, Figure 1-figure supplement 2**). Importantly,
134 the CiVDS-EPSC contributed 49% of the total EPSC (in amplitude) recorded in the
135 2Ca bath (CiVDS-EPSC + CDS-EPSC) during single-pulse stimulation, and this
136 increased to 87% during 10-Hz train stimulation (**Figures 1H, Figure 1-figure**
137 **supplement 2**), suggesting that, in contrast to CDS, CiVDS makes a dominant
138 contribution during sustained neural activity (**Figures 1I, Figure 1-figure supplement**
139 **2**).

140 In addition, we performed live-cell imaging of synaptophysin (Spy)-pHluorin in the
141 nerve terminals of DRG neurons co-cultured with DH neurons. Consistent with EPSC
142 recordings, an electrical field stimulation (20 Hz, 20 s) induced a notable increase of
143 the Spy-pHluorin signal in either 0Ca or 2Ca bath solution (*Figure 2A–C, Figure*
144 *2-video 1 and Figure 2-video 2*). Similar to electrophysiological results during 10-Hz
145 stimulation (*Figure 1-figure supplement 2C*), the peak amplitude of $\Delta F/F_0$ evoked in
146 0Ca solution was 77% of that evoked in 2Ca solution, further confirming the
147 dominant contribution of CiVDS during sustained neural activity (*Figure 2C*).
148 However, the same electrical stimulation triggered Spy-pHluorin exocytosis in
149 hippocampal nerve terminals only in 2Ca solution, but not 0Ca solution (*Figure 2D–F,*
150 *Figure 2-video 3 and Figure 2-video 4*). Thus, CiVDS mediates synaptic
151 transmission in co-cultured DRG and DH neurons.

152 **CiVDS-EPSC is mediated by glutamate release from presynaptic DRG neurons**

153 To determine whether the CiVDS-EPSC is mediated by presynaptic glutamate release,
154 we tested the effects of ionic glutamate receptor blockers (D-AP5 for NMDA receptor
155 and CNQX for AMPA receptor (Trussell, Zhang, & Raman, 1993; C. Wang et al.,
156 2016)). Three minutes of exposure to AP5 (50 μ M) and CNQX (10 μ M) diminished
157 the EPSCs in both the 0Ca and 2Ca solutions (*Figure 3A–B*). As a control, there was
158 only minimal run-down during repeated stimulation of CiVDS-EPSCs (*Figure*
159 *3-figure supplement 1*). Furthermore, 3-min treatment with 100 μ M cyclothiazide
160 (CTZ), a blocker of AMPA receptor desensitization (Fucile, Milei, & Eusebi, 2006),
161 greatly slowed the decay and increased the charge of the EPSC in both the 0Ca and

162 2Ca solutions (**Figure 3C-D**). Thus, the CiVDS-EPSC is mediated by synaptic
163 glutamate transmission in co-cultured DRG and DH neurons.

164 To determine whether DRG neurons are responsible for the presynaptic glutamate
165 release in CiVDS-EPSCs, we performed paired whole-cell recordings to examine the
166 specific synaptic transmission between the patched presynaptic DRG (current-clamp)
167 and postsynaptic DH neurons (voltage-clamp). EPSC traces were recorded in the
168 standard 2Ca bath within 1 min and 0Ca bath 5 min after whole-cell dialysis, in which
169 10 mM BAPTA was whole-cell dialyzed into the patched DRG neuron (**Figure 4A**) to
170 ensure the intracellular Ca²⁺-free condition (**Figure 4A**). A single pulse of current
171 injection (5 ms, 1000 pA) after break-in triggered an action potential in the
172 presynaptic DRG neuron, followed by an EPSC in the postsynaptic DH neuron in 2Ca
173 bath solution (**Figure 4B**). Strikingly, a notable EPSC signal (~40%) remained 5 min
174 after whole-cell dialysis even though the patched neurons were bathed in 1 mM
175 EGTA-containing Ca²⁺-free solution (**Figure 4B**). In contrast, similar Ca²⁺-free
176 treatment completely blocked the EPSCs in hippocampal neurons (**Figure 4C-D**).
177 Thus, CiVDS-mediated transmitter release from the presynaptic DRG neurons
178 contributes to EPSC signals in the postsynaptic DH neurons.

179 We next used an optogenetic approach to specifically activate DRG neurons by
180 expressing channelrhodopsin-2 (ChR2) in DRG neurons with AAV2/9 virus before the
181 co-culture with DH neurons (**Figure 4E-F**). The transient application of 475-nm light
182 evoked action potentials in ChR2-expressing DRG neurons (**Figure 4-figure**
183 **supplement 1**). Importantly, the light-activation of DRG neurons also induced EPSCs

184 in DH neurons bathed in either 0Ca or 2Ca solution, and these were fully abolished by
185 the blockade of ionic glutamate receptors with D-AP5 and CNQX (**Figure 4G**).
186 Together, these findings demonstrate that an action potential *per se* is able to directly
187 trigger presynaptic glutamate release independent of Ca²⁺ influx during the synaptic
188 transmission from presynaptic DRG terminals to postsynaptic central DH neurons.

189

190 **CiVDS-EPSC is mediated by SNARE complex and N-type Ca²⁺-channels**

191 To determine whether the CiVDS-EPSC is mediated by SNARE-dependent vesicular
192 exocytosis, we performed DRG neuron-restricted knockout of synaptobrevin 2
193 (Syb2/VAMP2) by infecting DRG neurons from homozygous floxed Syb2-null mice
194 with Cre recombinase-carrying AAV2/5 virus (**Figure 5A**). Western blots showed the
195 complete loss of Syb2 in DRG neurons infected with Cre virus (**Figure 5B**).
196 Strikingly, the CiVDS-EPSC in DRG–DH transmission was substantially reduced by
197 the Syb2-knockout (**Figure 5C**). Thus, similar to CiVDS in somatic secretion (Chai et
198 al., 2017), CiVDS-mediated presynaptic glutamate release occurs through
199 SNARE-dependent vesicular exocytosis.

200 We have shown that the N-type Ca²⁺ channel Cav2.2 serves as a voltage sensor for
201 CiVDS in the somata of DRG and superior cervical ganglion neurons, while the
202 L-type Ca²⁺ channel mediates CiVDS in adrenal slice chromaffin cells (Chai et al.,
203 2017; Huang et al., 2019). To determine the voltage sensor for CiVDS in synaptic
204 transmission of DRG-DH neurons, we blocked Cav2.2 with ω -conotoxin-GVIA
205 (GVIA, 1 μ M), which directly blocks the voltage-sensing ability of Cav2.2 (Chai et al.,

206 2017; Ellinor, Zhang, Horne, & Tsien, 1994; Yarotsky & Elmslie, 2009, 2010), and
207 found that both CiVDS- and CDS-mediated EPSCs were remarkably decreased
208 (*Figures 5D, Figure 5-figure supplement 1*). On the contrary, CiVDS-mediated
209 EPSCs were insensitive to Cd^{2+} , a well-known pore blocker of VGCCs (Chow, 1991;
210 Huang et al., 2019; Tang et al., 2014) (*Figure 5-figure supplement 2*), confirming that
211 the gating charge but not pore permeability is crucial for CiVDS-EPSCs. To further
212 confirm the essential role of Cav2.2 in CiVDS-EPSCs, we adopted an shRNA-based
213 knockdown (KD) approach. As validated previously (Chai et al., 2017), two
214 independent Cav2.2-targeting shRNAs (sh-1 and sh-2) were delivered into DRG
215 neurons by the AAV2/5 virus before co-culture with DH neurons (*Figure 5E*). Both
216 the CiVDS- and CDS-mediated EPSCs in DH neurons were substantially decreased
217 by Cav2.2-KD in presynaptic DRG neurons compared with those in control group
218 (*Figure 5F, Figure 5-figure supplement 3*). Together, these findings indicate that
219 Cav2.2 serves as a voltage sensor for CiVDS-mediated glutamate release during the
220 synaptic transmission from DRG to DH neurons.

221

222 **Discussion**

223 The classic view of neurotransmission is that impulse-induced presynaptic release
224 (both somatic and terminal) occurs exclusively *via* CDS (Felmy et al., 2003; Geppert
225 et al., 1994; Jackson & Chapman, 2006; Katz & Miledi, 1967; Meinrenken et al.,
226 2003; Neher & Zucker, 1993; Sudhof, 2012). In somatic secretion, the CDS-only
227 concept has recently been revised by a series of studies on CiVDS in peripheral

228 sensory and sympathetic neurons (Huang et al., 2019; Liu et al., 2011; Moya-Diaz et
229 al., 2019; Sforza et al., 2019; C. Zhang et al., 2004; C. Zhang & Zhou, 2002; Zheng et
230 al., 2009), including its functions and mechanisms (Chai et al., 2017). In the present
231 study, we show that CiVDS contributes to synaptic transmission in the central nervous
232 system: at synapses between presynaptic DRG terminals and postsynaptic central DH
233 neurons. The CiVDS-mediated EPSCs have a faster recycling rate and less short-term
234 depression than CDS-mediated EPSCs. Similar to somatic CiVDS, the machinery
235 governing CiVDS-mediated synaptic transmission includes Cav2.2 (voltage sensor)
236 and Syb2-SNARE (fusion pore) (**Figure 6**).

237 The major finding of the present work is that CiVDS contributes to the central
238 synaptic transmission between co-cultured presynaptic DRG and postsynaptic DH
239 neurons. This is supported by the following evidence: (1) EPSCs were recorded in
240 DRG-DH (**Figure 1A,C**) but not hippocampal neurons (**Figure 1B**) in 0Ca solution;
241 (2) field stimulation triggered a $[Ca^{2+}]_i$ rise only in Ca^{2+} -containing solution (**Figures**
242 **1A, Figure 1-figure supplement 1**); (3) in 2Ca solution, BAPTA reduced the EPSC
243 amplitude to that in 0Ca (**Figure 1C-D**); (4) the evoked CiVDS-EPSCs were
244 abolished by antagonists against AMPA receptors (CNQX) and NMDA receptors
245 (AP5) (Trussell et al., 1993; C. Wang et al., 2016) (**Figure 3A-B**); (5) the decay of
246 evoked CiVDS-EPSCs was greatly slowed by the AMPA receptor enhancer CTZ
247 (Fucile et al., 2006) (**Figure 3C-D**); (6) Spy-pHluorin live-imaging confirmed CiVDS
248 from the presynaptic terminals of DRG neurons but not hippocampal neurons (**Figure**
249 **2, Figure 2-video 1-4**); (7) paired patch-clamp recordings revealed that EPSCs

250 between DRG-DH neurons were independent of extracellular and intracellular Ca^{2+} ,
251 while the EPSCs in hippocampal neurons were completely blocked in the 0Ca
252 condition (**Figure 4A-D**); (8) optogenetic stimulation of DRG neurons triggered
253 EPSCs in either 0Ca or 2Ca solution, confirming that presynaptic glutamate release
254 from DRG neurons is responsible for both the CiVDS-EPSCs and CDS-EPSCs
255 recorded in DH neurons (**Figure 4E-G**); (9) SNARE is the CiVDS fusion machinery
256 of the EPSCs, which were attenuated by knockout of the SNARE protein Syb2 in
257 DRG neurons (**Figure 5A-C**); and (10) Cav2.2 is the voltage-sensor of
258 CiVDS-EPSCs, as they were attenuated by either RNAi knockdown or an antagonist
259 GVIA, which inhibits the voltage-sensor of Cav2.2 (Chai et al., 2017; Ellinor et al.,
260 1994; Yarotsky & Elmslie, 2009, 2010), but were insensitive to open Ca^{2+} channel
261 blocker Cd^{2+} (Chow, 1991; Huang et al., 2019; Tang et al., 2014) (**Figures 5D-F**,
262 **Figure 5-figure supplement 2**). Together, CiVDS contributes to the EPSCs between
263 DRG and DH neurons in physiological solution and in response to physiological
264 stimulation.

265 The second finding is that both CiVDS and CDS make essential and
266 complementary contributions to the total EPSC (CDS + CiVDS) of DRG-DH
267 synaptic transmission under physiological conditions: 2 mM Ca^{2+} bath solution and
268 ≤ 20 Hz stimulation (Fang et al., 2005; Xu et al., 2000; Zheng et al., 2009). This is
269 supported by the following evidence: (1) compared to the CDS-EPSC, the
270 CiVDS-EPSC had a faster vesicle recycling rate (**Figure 1E-F**) and less short-term
271 depression (**Figure 1G-H**); (2) CDS [EPSC(2Ca) – EPSC(0Ca)] and CiVDS

272 [EPSC(0Ca)] contributed similarly (~50% each) to the total EPSC during synaptic
273 transmission following single-pulse/low-frequency stimulation (≤ 0.2 Hz) (**Figure**
274 **1D,F**); (3) CiVDS became dominant (~87%) in the total EPSC following “painful”
275 high-frequency stimulation (10-20 Hz) (Fang et al., 2005; Xu et al., 2000; Zheng et al.,
276 2009), as CDS was attenuated more than CiVDS in the total EPSC (**Figure 1G-I**) due
277 to much slower vesicle recycling of the CDS-EPSC (Neher & Sakaba, 2008; L. Y.
278 Wang, Neher, & Taschenberger, 2008; B. Zhang et al., 2011); (4) single-pulses or low
279 frequency (≤ 0.2 Hz) triggered both CDS and CiVDS in synaptic release (**Figure 1**),
280 while only CiVDS (C. Zhang & Zhou, 2002; Zheng et al., 2009) but not CDS (Huang
281 et al., 2019; Liu et al., 2011; Zheng et al., 2009) was triggered during somatic
282 secretion; and (5) a “painful” burst of pulses (10-20 Hz) (Fang et al., 2005; Xu et al.,
283 2000; Zheng et al., 2009) triggered both CiVDS and CDS in synaptic transmission
284 (**Figure 1**), as well as somatic exocytosis (C. Zhang & Zhou, 2002; Zheng et al.,
285 2009). Together, CiVDS and CDS make essential and complementary contributions to
286 both synaptic EPSCs (**Figure 1**) and somatic transmitter release (Chai et al., 2017) in
287 the DRG-DH sensory system.

288 The present study reported CiVDS-mediated synaptic transmission in a central
289 synapse between DRG and DH neurons. In contrast, release from the presynaptic
290 terminal of the calyx of Held is abolished after blocking Ca^{2+} influx (Felmy et al.,
291 2003). Future work is needed to determine: (1) whether CiVDS-EPSCs occur in the
292 synaptic transmission of other neural circuits; (2) whether CiVDS-IPSCs exist; (3)
293 whether CiVDS-EPSCs occur in brain slices and *in vivo*; and (4) the physiological

294 relevance of CiVDS-EPSCs.

295 In summary, the present work extends the occurrence of CiVDS from peripheral
296 neuronal somata and neuroendocrine cells to a central presynaptic terminal, and
297 demonstrates CiVDS-EPSCs in a rat/mouse model of cultured DRG–DH neurons,
298 implying potential physiological roles of CiVDS in synaptic transmission in other
299 mammalian neural circuits.

300

301 **Materials and methods**

302 **Animals**

303 The use and care of animals was approved and directed by the Institutional Animal
304 Care and Use Committee of Peking University and the Association for Assessment
305 and Accreditation of Laboratory Animal Care. We used CRISPR/Cas9-mediated
306 one-step genomic engineering to generate Synaptobrevin-2 floxed mice (Yang et al.,
307 2013). A mixture of guide RNAs (CTCTGGTGATAGGCGGATCCAGG,
308 AGGGTTCCTAGACGAACACCAGG), the corresponding donor DNA and the Cas9
309 protein was micro-injected into the fertilized eggs, followed by embryonic
310 transplantation. Two LoxP sites were inserted into the 5' intron of exon 3 and 3' intron
311 of exon 4 in mouse synaptobrevin-2 gene donor fragment (Gene ID: 22318). All
312 animals were housed in an animal facility under a 12-h light/dark cycle at $22 \pm 2^\circ\text{C}$
313 with food and water available *ad libitum*. Sprague-Dawley rats were used for all
314 experiments except that floxed Syb2-null mice were used for Syb2-KO experiments.

315 **Cell culture**

316 Three to four-day old postnatal Sprague-Dawley rats or floxed Syb2-null mice were
317 used for the culture of dorsal root ganglion (DRG) neurons and 15–16 day embryos of
318 Sprague-Dawley rats were used for the culture of dorsal horn (DH) neurons. Postnatal
319 day 0 Sprague-Dawley rats were used for the culture of hippocampal neurons.

320 DRG isolation and neuronal culture were performed as previously described (Chai
321 et al., 2017). DRG ganglia were dissected from the spine and placed in cold L15
322 medium (Gibco). After removing attached tissue, the ganglia were cut into several
323 pieces and incubated in Dulbecco's modified Eagle's medium (DMEM)/F12 (Gibco)
324 containing trypsin (0.2- 0.3 mg/ml) and collagenase (1 mg/ml) for 40 min at 37°C
325 under 5% CO₂. After that, the pieces were washed twice with 2 ml DMEM/F12 and
326 dissociated into single cells by 8–10 bouts of trituration. For confocal imaging, cells
327 were collected and transfected with Synaptophysin (Spy)-pHluorin plasmid (a kind
328 gift from Dr. G. Miesenböck, University of Oxford) by using the NeonTM (100- μ l)
329 electroporation system (MPK10096, Invitrogen). Then the cell suspension was placed
330 on 0.1% poly-L-lysine pretreated coverslips and maintained in Neurobasal
331 supplemented with 2% B27 and 0.5 mM L-glutamine (all from Gibco).

332 DH neurons were isolated and cultured as previously described (Zheng et al., 2009).
333 The spinal cord was dissected from 15–16-day embryos and placed in cold D-Hanks
334 solution. After removing attached tissue, the dorsal spinal cord was incubated in 0.25%
335 trypsin solution for 15 min at 37°C under 5% CO₂. After that, the dorsal cord was
336 washed twice with 2 ml Neurobasal supplemented with 2% B27 and 0.5 mM
337 L-glutamine (all from Gibco) and dissociated into single cells by 8–10 bouts of

338 trituration. To co-culture DRG and DH neurons, the suspension of DH neurons was
339 evenly placed onto pre-cultured DRG neurons. All cells were maintained in
340 Neurobasal supplemented with 2% B27, 0.5 mM L-glutamine (all from Gibco), 10
341 ng/ml nerve growth factor (NGF), 50 ng/ml brain-derived neurotrophic factor (BDNF),
342 50 ng/ml glial cell line-derived neurotrophic factor (GDNF), and 5 μ M cytosine
343 arabinoside. The mixture of NGF, BDNF, and GDNF helped to maintain CiVDS
344 for >2 weeks. The neurons were used between days 10-12 after the start of co-culture.

345 For hippocampal cultures, hippocampal neurons were prepared as previously
346 described (C. Wang et al., 2018). Briefly, hippocampi were dissected from neonatal
347 rats and placed in cold D-Hanks solution. After removing attached tissue, the
348 hippocampi were digested in 0.25 % trypsin for 15 min at 37°C under 5% CO₂. After
349 that, the tissue was washed twice with 2 ml Neurobasal supplemented with 2% B27
350 and 0.5 mM L-glutamine (all from Gibco), and dissociated by 8–10 bouts of
351 trituration. Then the cells were placed on 0.1% poly-L-lysine-coated coverslips and
352 maintained in DMEM (Gibco) supplemented with 10% FBS for 3 h, which was then
353 replaced by Neurobasal supplemented with 2% B27 and 0.5 mM L-glutamine.
354 Experiments were performed between days 14-16 after the start of culture. For
355 confocal imaging, cultures at day 5 were transfected with Spy-pHluorin plasmid by
356 using a calcium-phosphate transfection method. Briefly, plasmids in a 250 mM CaCl₂
357 solution were slowly added to Hank's balanced salt solution (HBSS) and incubated at
358 room temperature for 25 min. The mixture was then added to the culture and
359 incubated for 15 min. The cells were washed with MgCl₂-containing medium and then

360 maintained in the original medium. Confocal imaging was performed at day 13-14.

361 **Virus infection**

362 For virus infection, the virus was added to the culture solution at the beginning of
363 DRG neuronal culture. After 3 days, the virus-containing culture medium was fully
364 replaced and then the DH neurons were co-cultured with the DRG neurons. The
365 adeno-associated virus vector carrying CAG-hChR2(H134R)-mCherry (AAV2/9) was
366 used for optogenetics and CAG-EGFP-2A-Cre (AAV2/5) for Syb2-knockout. For
367 Cav2.2 knockdown, the nucleotide target sequences GG ACA TTT CTG CAA GCC
368 TTA A (shCav2.2-1) and GC TAC TTC CGG TCT TCC TTC A (shCav2.2-2) were
369 integrated into adeno-associated virus (AAV2/5) to silence the expression of Cav2.2.
370 All the viruses were from Shanghai Heyuan Biotech (China).

371 **Electrophysiology**

372 Excitatory postsynaptic currents (EPSCs) were recorded under the whole-cell
373 configuration using an EPC10/2 amplifier controlled by Patchmaster software (HEKA
374 Elektronik) as described previously (B. Zhang et al., 2011; Zheng et al., 2009). The
375 membrane potential was clamped at -70 mV, and pipette resistance was controlled to
376 ~ 10 M Ω for EPSC recordings. The standard external bath solution contained (in mM):
377 150 NaCl, 5 KCl, 2.5 CaCl₂, 1 MgCl₂, 10 H-HEPES, and 10 D-glucose, pH 7.4. The
378 Ca²⁺-free solution for CiVDS recording was the same, except that 2.5 mM Ca²⁺ was
379 replaced by 1 mM EGTA. For EPSC recording, 100 μ M picrotoxin was added to the
380 bath to block IPSCs (inhibitory postsynaptic currents). The standard intracellular
381 pipette solution contained (in mM): 145 K-gluconate, 5 KCl, 4 MgCl₂·6H₂O, 10

382 H-HEPES, 5 EGTA, and 2 QX314, pH 7.2. Standard intracellular solution with CsCl
383 containing (in mM) 153 CsCl, 1 MgCl₂, 10 H-HEPES, 4 Mg-ATP, 5 QX314, pH7.2
384 was used for a stable recording in Syb2-KO and optogenetic experiments. For EPSC
385 recordings, local electrical field or light stimulation was applied. Field electrical
386 stimulation (Estim) was used to evoke action potentials *via* a laboratory-made bipolar
387 microelectrode (150 μm in diameter) connected to an electronic stimulator (Nihon
388 Kohden, SEN-3201) (B. Zhang et al., 2011).

389 In paired patch-clamp recordings, the presynaptic DRG neuron was in whole-cell
390 current-clamp mode and the postsynaptic dorsal horn neuron was in whole-cell
391 voltage-clamp mode. For the current-clamp of DRG neurons, the intracellular solution
392 contained (in mM) 135 K-gluconate (115 when adding 10 mM BAPTA), 5 KCl, 4
393 MgCl₂, 3 MgATP, 0.3 Na₂GTP, and 10 Na₂-phosphocreatine, 10 HEPES, pH 7.2. For
394 the voltage-clamp DH neuron, standard intracellular solution (but CsCl replacing KCl)
395 was used. For light stimulation, 475-nm light was generated by a laser (VD-III A,
396 Beijing Viasho Technology, China).

397 All recordings were made at room temperature (25°C). Igor software (Wavemetrics,
398 Lake Oswego, OR) was used for all offline data analysis. Series conductance and
399 membrane conductance were used to monitor the seal condition during patch-clamp
400 recordings.

401 **Ca²⁺ imaging**

402 Ca²⁺ imaging was conducted as described previously (Huang et al., 2019; Shang et al.,
403 2016). Cytosolic Ca²⁺ was measured with the Ca²⁺ indicator Cal-520 (21130, AAT

404 Bioquest). Co-cultured DRG and DH neurons were loaded with 0.5 μM Cal-520 AM
405 for 30 min at 37°C and then washed 3 times with 2 mM Ca^{2+} solution at room
406 temperature. Then the cells were electrically simulated and imaged on an inverted
407 confocal microscope (LSM710, Zeiss). The fluorescent signal was captured by
408 excitation with a 488-nm laser and emission at 500–560 nm. Fluorescence intensity
409 values from the images were calculated and analyzed using ImageJ. The cutoff for
410 selection (5 a.u.) was 1.5-fold that of the full-width at half-maximum of the Gaussian
411 distribution of fluorescence noise.

412 **Confocal live-imaging**

413 Time-lapse images were captured at 0.5 s interval through the inverted confocal
414 microscope (LSM710, Zeiss) with a 63 x oil-immersion objective lens (Zeiss). The
415 fluorescent signal was captured by excitation with a 488-nm laser and emission at
416 500–560 nm at room temperature bathed in Ca^{2+} -free or standard external solution.
417 Electrical field stimulation was applied via an electrical stimulator (Nihon Kohden,
418 SEN-3201). Fluorescence changes at individual boutons were monitored over time
419 and calculated as $\Delta F/F_0$. Images were acquired for more than 200 s in total. The first
420 30 s before stimulation was used to establish a baseline. Data were analyzed offline
421 with ImageJ.

422 **Protein preparation and western blotting**

423 Cells were washed with phosphate-balanced saline (PBS) and homogenized on ice
424 with lysate buffer (RIPA; C1503, Beijing Applygen Technologies Inc.), 1 mM PMSF,
425 and 2% proteinase inhibitor (539,134; Calbiochem). The homogenates were

426 centrifuged at 13,000 rpm for 10 min at 4°C and the supernatants were collected and
427 boiled in SDS-PAGE buffer. Proteins were electrophoresed and transferred to
428 nitrocellulose filter membranes (Pall Life Sciences). The membranes were blocked for
429 1 h with PBS containing 0.1% Tween-20 (v/v) and 5% fat-free milk (w/v), then
430 incubated with primary antibodies at 4°C overnight in PBST containing 2% bovine
431 serum albumin. After washing with 0.1% Tween-20 containing PBS (PBST), they
432 were then incubated with secondary antibodies at room temperature for 1 h. Blots
433 were scanned with an Odyssey infrared imaging system (LI-COR Biosciences) and
434 quantified with ImageJ (National Institutes of Health, Bethesda, MD). The primary
435 antibodies used were anti-Syb2 (104202, SYSY) and β -actin (A5316, Sigma). The
436 secondary antibodies were IRDye 800CW goat anti-rabbit IgG (LIC-926-32211) and
437 IRDye 680CW goat anti-mouse IgG (LIC-926-32220), both from LI-COR
438 Biosciences.

439 **Statistical analysis**

440 All experiments were performed with controls side-by-side and in random order, and
441 were replicated at least three times. All data were collected at least every 2 weeks
442 within 3 months window to maintain the stability of a data set. Sample sizes are
443 consistent with those reported in similar studies. Multiple recordings from one cell
444 with the identical stimulus protocol were considered as technical replications, which
445 were averaged to generate a single biological replication representing value/data from
446 one cell. No samples or recordings that provided successful measurements were
447 excluded from analysis. Data are shown as the mean \pm s.e.m. All the data were tested

448 for normality by Shapiro-Wilk test before the statistical analysis. If the data passed the
449 normality test, two-tailed Student's *t* test was applied for comparison between two
450 unpaired groups and the paired Student's *t* test was used for comparison between two
451 matched groups. If the data did not pass normality, Mann-Whitney test was applied
452 for comparison between two unpaired groups, Wilcoxon matched-pairs signed rank
453 test (Wilcoxon test) was applied for two matched groups and the Kruskal-Wallis test
454 followed by Dunn's multiple comparisons test was used when multiple groups were
455 compared with one variable. All tests were conducted using Prism V7.0 (GraphPad
456 Software, Inc.) and SPSS 20.0 (Statistical Package for the Social Sciences).
457 Significant differences were accepted at $p < 0.05$.

458 **Acknowledgements**

459 We thank Drs. Mengping Wei and Chen Zhang (Capital Medical University) for
460 advices on EPSC recordings and virus transfection *in vivo*, Jianguo Gu (UA
461 Birmingham), Kun Yang (Jiangsu University) and Luyang Wang (Toronto University)
462 for helpful discussions, and Iain C. Bruce (Peking University) for reading the
463 manuscript. This work was supported by National Natural Science Foundation of
464 China (31930061, 21790394, 31761133016, 31821091, 31330024, 31171026,
465 31327901, 32171233, 31670843 and 21790390), the National Key Research and
466 Development Program of China (2016YFA0500401), the Shaanxi Natural Science
467 Funds for Distinguished Young Scholars of China (2019JC-07), the Innovation
468 Capability Support Program of Shaanxi Province, China (2021TD-37), and the China
469 Postdoctoral Science Foundation (2020M680211, 2021T140014).

470

471 **Additional information**

472 **Funding**

Funder	Grant reference number	Author
National Natural Science Foundation of China	31930061	Zhuan Zhou
National Natural Science Foundation of China	21790394	Zhuan Zhou
National Natural Science Foundation of China	31761133016	Zhuan Zhou
National Natural Science Foundation of China	31821091	Zhuan Zhou
National Natural Science Foundation of China	31330024	Zhuan Zhou
National Natural Science Foundation of China	31171026	Zhuan Zhou
National Natural Science Foundation of China	31327901	Zhuan Zhou
National Natural Science Foundation of China	32171233	Changhe Wang
National Natural Science Foundation of China	31670843	Changhe Wang
National Natural Science Foundation of China	21790390	Zhuan Zhou

National Key Research and Development Program of China	2016YFA0500401	Zhuan Zhou
Shaanxi Natural Science Funds for Distinguished Young Scholars of China	2019JC-07	Changhe Wang
Innovation Capability Support Program of Shaanxi Province, China	2021TD-37	Changhe Wang
China Postdoctoral Science Foundation	2020M680211	Rong Huang
China Postdoctoral Science Foundation	2021T140014	Rong Huang
The funders had no role in study design, data collection and interpretation, or the decision to submit the work for publication.		

473

474 **Author contributions**

475 Y.W., R.H., X.D. and Y.H. performed and analyzed the experiments with the help of

476 Y.X., J.L., X.J., X.W., Z.Q., Y.L., B.L. and F.Z.; Y.Z. and P.C. generated floxed

477 Syb2-null mice; Z.Z., Z.C. and C.W. designed the work and wrote the manuscript with

478 inputs from all authors. Z.Z. supervised the project.

479

480 **References**

- 481 Artalejo, C. R., Elhamdani, A., & Palfrey, H. C. (2002). Sustained stimulation shifts the
482 mechanism of endocytosis from dynamin-1-dependent rapid endocytosis to clathrin-
483 and dynamin-2-mediated slow endocytosis in chromaffin cells. *Proc Natl Acad Sci U S*
484 *A*, *99*(9), 6358-6363. doi: 10.1073/pnas.082658499
- 485 Augustine, G. J., Charlton, M. P., & Smith, S. J. (1987). Calcium action in synaptic transmitter
486 release. *Annu Rev Neurosci*, *10*, 633-693. doi:
487 10.1146/annurev.ne.10.030187.003221
- 488 Chai, Z., Wang, C., Huang, R., Wang, Y., Zhang, X., Wu, Q., . . . Zhou, Z. (2017). Cav2.2 gates
489 calcium-independent but voltage-dependent secretion in mammalian sensory neurons.
490 *Neuron*, *96*(6), 1317-1326 e1314. doi: 10.1016/j.neuron.2017.10.028
- 491 Chow, R. H. (1991). Cadmium block of squid calcium currents. Macroscopic data and a kinetic
492 model. *J Gen Physiol*, *98*(4), 751-770. doi: 10.1085/jgp.98.4.751
- 493 Ellinor, P. T., Zhang, J. F., Horne, W. A., & Tsien, R. W. (1994). Structural determinants of the
494 blockade of n-type calcium channels by a peptide neurotoxin. *Nature*, *372*(6503),
495 272-275. doi: 10.1038/372272a0
- 496 Fang, X., McMullan, S., Lawson, S. N., & Djouhri, L. (2005). Electrophysiological differences
497 between nociceptive and non-nociceptive dorsal root ganglion neurones in the rat in
498 vivo. *J Physiol*, *565*(Pt 3), 927-943. doi: 10.1113/jphysiol.2005.086199
- 499 Felmy, F., Neher, E., & Schneggenburger, R. (2003). The timing of phasic transmitter release
500 is ca²⁺-dependent and lacks a direct influence of presynaptic membrane potential.
501 *Proc Natl Acad Sci U S A*, *100*(25), 15200-15205. doi:

- 502 10.1073/pnas.24332761002433276100 [pii]
- 503 Ferguson, S. M., Brasnjo, G., Hayashi, M., Wolfel, M., Collesi, C., Giovedi, S., . . . De Camilli,
504 P. (2007). A selective activity-dependent requirement for dynamin 1 in synaptic vesicle
505 endocytosis. *Science*, *316*(5824), 570-574. doi: 10.1126/science.1140621
- 506 Fucile, S., Miledi, R., & Eusebi, F. (2006). Effects of cyclothiazide on glur1/ampa receptors.
507 *Proc Natl Acad Sci U S A*, *103*(8), 2943-2947. doi: 0511063103
508 [pii]10.1073/pnas.0511063103
- 509 Geppert, M., Goda, Y., Hammer, R. E., Li, C., Rosahl, T. W., Stevens, C. F., & Sudhof, T. C.
510 (1994). Synaptotagmin i: A major ca²⁺ sensor for transmitter release at a central
511 synapse. *Cell*, *79*(4), 717-727. doi: 10.1016/0092-8674(94)90556-8
- 512 Hopfield, J. J. (1995). Pattern recognition computation using action potential timing for
513 stimulus representation. *Nature*, *376*(6535), 33-36. doi: 10.1038/376033a0
- 514 Huang, R., Wang, Y., Li, J., Jiang, X., Li, Y., Liu, B., . . . Zhou, Z. (2019). Ca(2+)-independent
515 but voltage-dependent quantal catecholamine secretion (civds) in the mammalian
516 sympathetic nervous system. *Proc Natl Acad Sci U S A*. doi: 201902444
517 [pii]10.1073/pnas.19024441161902444116 [pii]
- 518 Jackson, M. B., & Chapman, E. R. (2006). Fusion pores and fusion machines in ca²⁺-triggered
519 exocytosis. *Annu Rev Biophys Biomol Struct*, *35*, 135-160. doi:
520 10.1146/annurev.biophys.35.040405.101958
- 521 Jahn, R., & Scheller, R. H. (2006). Snares--engines for membrane fusion. *Nat Rev Mol Cell*
522 *Biol*, *7*(9), 631-643. doi: 10.1038/nrm2002
- 523 Katz, B., & Miledi, R. (1967). Ionic requirements of synaptic transmitter release. *Nature*,

- 524 215(5101), 651. doi: 10.1038/215651a0
- 525 Liu, T., Shang, S. J., Liu, B., Wang, C. H., Wang, Y. S., Xiong, W., . . . Zhou, Z. (2011). Two
526 distinct vesicle pools for depolarization-induced exocytosis in somata of dorsal root
527 ganglion neurons. *J Physiol*, 589(Pt 14), 3507-3515. doi:
528 10.1113/jphysiol.2011.208777
- 529 Meinrenken, C. J., Borst, J. G., & Sakmann, B. (2003). Local routes revisited: The space and
530 time dependence of the ca²⁺ signal for phasic transmitter release at the rat calyx of
531 held. *J Physiol*, 547(Pt 3), 665-689. doi: 10.1113/jphysiol.2002.0327142002.032714
532 [pii]
- 533 Moya-Diaz, J., Bayones, L., Montenegro, M., Cardenas, A. M., Koch, H., Doi, A., & Marengo, F.
534 D. (2019). Ca²⁺ -independent and voltage-dependent exocytosis in mouse
535 chromaffin cells. *Acta Physiol (Oxf)*, e13417. doi: 10.1111/apha.13417
- 536 Nanou, E., & Catterall, W. A. (2018). Calcium channels, synaptic plasticity, and
537 neuropsychiatric disease. *Neuron*, 98(3), 466-481. doi: 10.1016/j.neuron.2018.03.017
- 538 Neher, E., & Sakaba, T. (2008). Multiple roles of calcium ions in the regulation of
539 neurotransmitter release. *Neuron*, 59(6), 861-872. doi: 10.1016/j.neuron.2008.08.019
- 540 Neher, E., & Zucker, R. S. (1993). Multiple calcium-dependent processes related to secretion
541 in bovine chromaffin cells. *Neuron*, 10(1), 21-30. doi: Doi
542 10.1016/0896-6273(93)90238-M
- 543 Parnas, I., & Parnas, H. (2010). Control of neurotransmitter release: From ca²⁺ to voltage
544 dependent g-protein coupled receptors. *Pflugers Arch*, 460(6), 975-990. doi:
545 10.1007/s00424-010-0872-7

- 546 Sabatini, B. L., & Regehr, W. G. (1996). Timing of neurotransmission at fast synapses in the
547 mammalian brain. *Nature*, *384*(6605), 170-172. doi: 10.1038/384170a0
- 548 Sforza, L., Franciolini, F., & Catacuzzeno, L. (2019). Ca²⁺-dependent and Ca²⁺-
549 -independent somatic release from trigeminal neurons. *J Cell Physiol*, *234*(7),
550 10977-10989. doi: 10.1002/jcp.27901
- 551 Shang, S., Zhu, F., Liu, B., Chai, Z., Wu, Q., Hu, M., . . . Zhou, Z. (2016). Intracellular trpa1
552 mediates Ca²⁺ release from lysosomes in dorsal root ganglion neurons. *J Cell Biol*,
553 *215*(3), 369-381. doi: 10.1083/jcb.201603081
- 554 Sollner, T., Whiteheart, S. W., Brunner, M., Erdjument-Bromage, H., Geromanos, S., Tempst,
555 P., & Rothman, J. E. (1993). Snap receptors implicated in vesicle targeting and fusion.
556 *Nature*, *362*(6418), 318-324. doi: 10.1038/362318a0
- 557 Sudhof, T. C. (2012). Calcium control of neurotransmitter release. *Cold Spring Harb Perspect*
558 *Biol*, *4*(1), a011353. doi: 10.1101/cshperspect.a011353a011353
559 [pii]cshperspect.a011353 [pii]
- 560 Tang, L., Gamal El-Din, T. M., Payandeh, J., Martinez, G. Q., Heard, T. M., Scheuer, T., . . .
561 Catterall, W. A. (2014). Structural basis for Ca²⁺ selectivity of a voltage-gated calcium
562 channel. *Nature*, *505*(7481), 56-61. doi: 10.1038/nature12775
- 563 Trussell, L. O., Zhang, S., & Raman, I. M. (1993). Desensitization of ampa receptors upon
564 multiquantal neurotransmitter release. *Neuron*, *10*(6), 1185-1196. doi:
565 10.1016/0896-6273(93)90066-z
- 566 Wang, C., Kang, X., Zhou, L., Chai, Z., Wu, Q., Huang, R., . . . Zhou, Z. (2018).
567 Synaptotagmin-11 is a critical mediator of parkin-linked neurotoxicity and parkinson's

- 568 disease-like pathology. *Nat Commun*, *9*(1), 81. doi: 10.1038/s41467-017-02593-y
- 569 Wang, C., Wang, Y., Hu, M., Chai, Z., Wu, Q., Huang, R., . . . Zhou, Z. (2016).
570 Synaptotagmin-11 inhibits clathrin-mediated and bulk endocytosis. *EMBO Rep*, *17*(1),
571 47-63. doi: 10.15252/embr.201540689
- 572 Wang, L. Y., Neher, E., & Taschenberger, H. (2008). Synaptic vesicles in mature calyx of held
573 synapses sense higher nanodomain calcium concentrations during action
574 potential-evoked glutamate release. *J Neurosci*, *28*(53), 14450-14458. doi:
575 10.1523/JNEUROSCI.4245-08.200828/53/14450 [pii]
- 576 Wu, Q., Zhang, Q., Liu, B., Li, Y., Wu, X., Kuo, S., . . . Zhou, Z. (2019). Dynamin 1 restrains
577 vesicular release to a subquantal mode in mammalian adrenal chromaffin cells. *J*
578 *Neurosci*, *39*(2), 199-211. doi: 10.1523/JNEUROSCI.1255-18.2018
- 579 Xu, G. Y., Huang, L. Y., & Zhao, Z. Q. (2000). Activation of silent mechanoreceptive cat c and
580 adelta sensory neurons and their substance p expression following peripheral
581 inflammation. *J Physiol*, *528 Pt 2*, 339-348. doi: 10.1111/j.1469-7793.2000.00339.x
- 582 Yang, H., Wang, H., Shivalila, C. S., Cheng, A. W., Shi, L., & Jaenisch, R. (2013). One-step
583 generation of mice carrying reporter and conditional alleles by crispr/cas-mediated
584 genome engineering. *Cell*, *154*(6), 1370-1379. doi: 10.1016/j.cell.2013.08.022
- 585 Yarotskyy, V., & Elmslie, K. S. (2009). Omega-conotoxin gvia alters gating charge movement
586 of n-type (cav2.2) calcium channels. *J Neurophysiol*, *101*(1), 332-340. doi:
587 10.1152/jn.91064.2008
- 588 Yarotskyy, V., & Elmslie, K. S. (2010). Interference between two modulators of n-type (cav2.2)
589 calcium channel gating demonstrates that omega-conotoxin gvia disrupts open state

590 gating. *Biochim Biophys Acta*, 1798(9), 1821-1828. doi:
591 10.1016/j.bbamem.2010.05.004

592 Zhang, B., Sun, L., Yang, Y. M., Huang, H. P., Zhu, F. P., Wang, L., . . . Zhou, Z. (2011). Action
593 potential bursts enhance transmitter release at a giant central synapse. *J Physiol*,
594 589(Pt 9), 2213-2227. doi: 10.1113/jphysiol.2010.200154jphysiol.2010.200154 [pii]

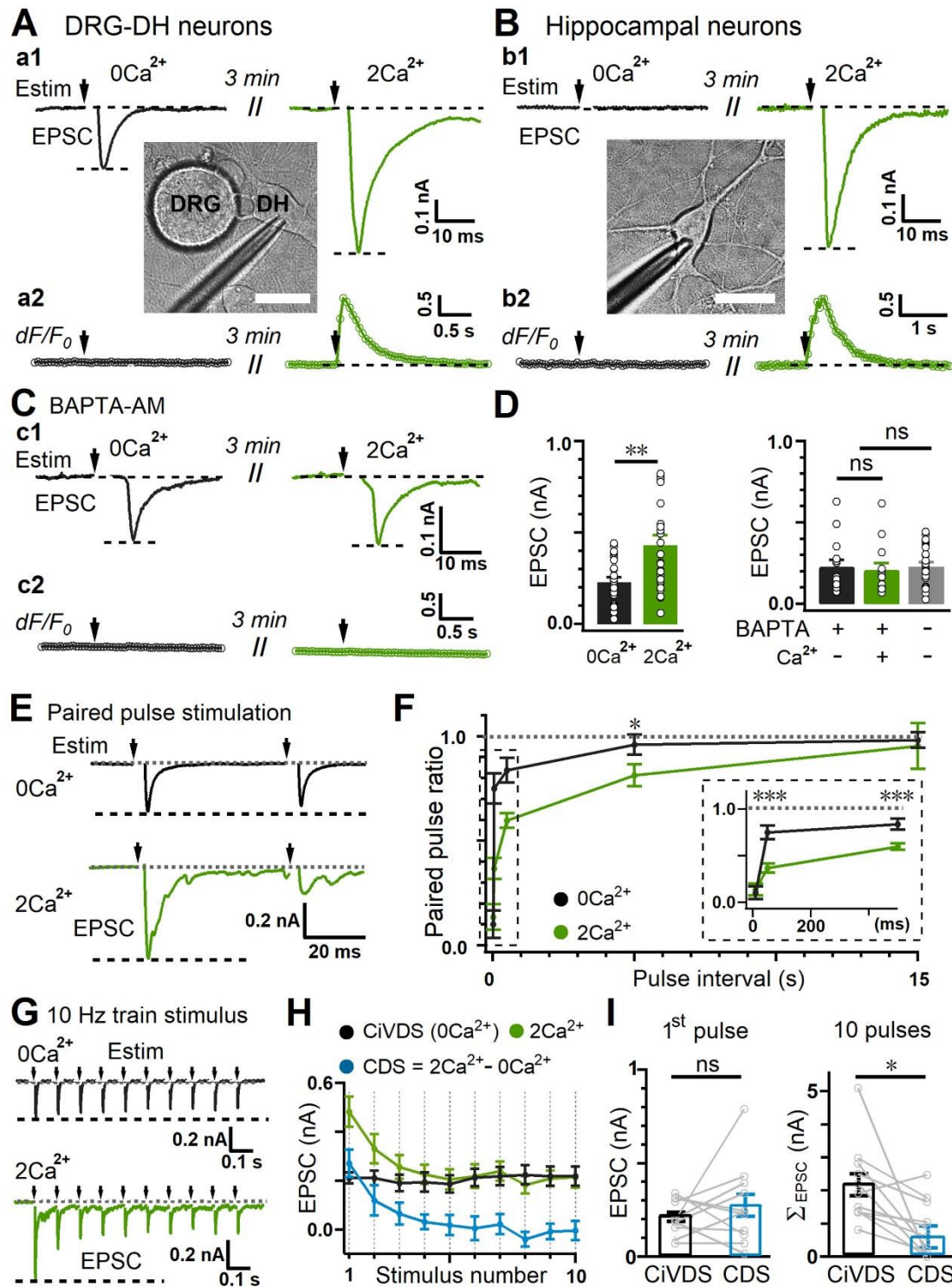
595 Zhang, C., Xiong, W., Zheng, H., Wang, L., Lu, B., & Zhou, Z. (2004). Calcium- and
596 dynamin-independent endocytosis in dorsal root ganglion neurons. *Neuron*, 42(2),
597 225-236. doi: 10.1016/s0896-6273(04)00189-8

598 Zhang, C., & Zhou, Z. (2002). Ca(2+)-independent but voltage-dependent secretion in
599 mammalian dorsal root ganglion neurons. *Nat Neurosci*, 5(5), 425-430. doi:
600 10.1038/nn845

601 Zheng, H., Fan, J., Xiong, W., Zhang, C., Wang, X. B., Liu, T., . . . Zhou, Z. (2009). Action
602 potential modulates ca²⁺-dependent and ca²⁺-independent secretion in a sensory
603 neuron. *Biophys J*, 96(6), 2449-2456. doi:
604 10.1016/j.neuron.2017.10.02810.1016/j.bpj.2008.11.037

605

606



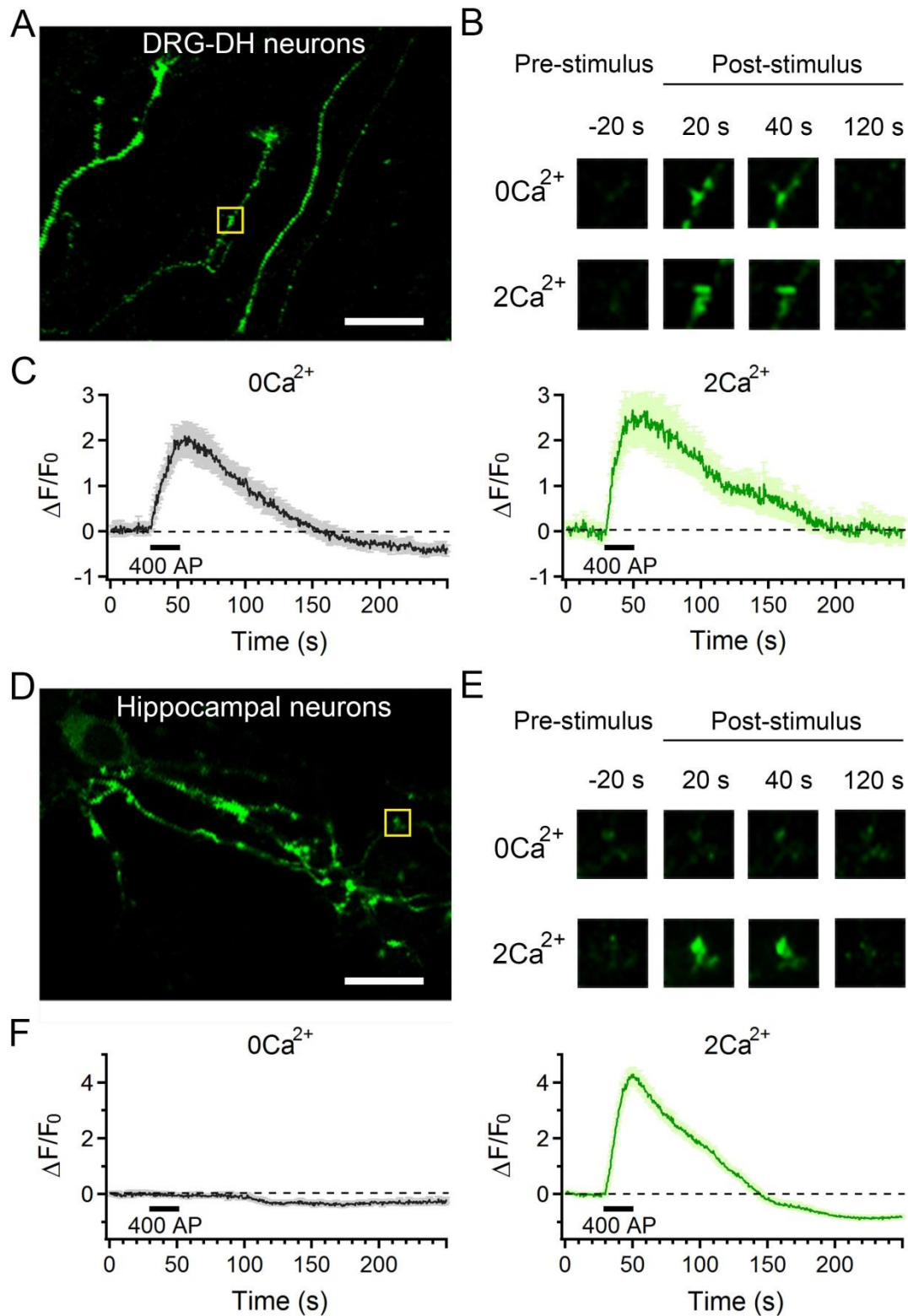
607 **Figure 1.** Ca^{2+} -independent but voltage-dependent synaptic neurotransmission in
 608 co-cultured DRG-DH neurons. (A) (a1) Whole-cell current recording of evoked EPSC
 609 signals in response to local electrical field stimulation (Estim, arrows) from a
 610 postsynaptic dorsal horn (DH) neuron co-cultured with presynaptic dorsal root

611 ganglion (DRG) neurons in Ca^{2+} -free (0Ca^{2+} , black) and 2 mM Ca^{2+} bath (2Ca^{2+} ,
612 green); (a2), evoked intracellular Ca^{2+} signals (dF/F_0) in a DRG neuron; inset,
613 micrograph showing the setup for EPSC recording from co-cultured DRG-DH
614 neurons (scale bar, 20 μm). (B) (b1) Evoked EPSCs from cultured hippocampal
615 neurons in Ca^{2+} -free (black) and 2 mM Ca^{2+} -containing solution (green); (b2) evoked
616 intracellular Ca^{2+} signals (dF/F_0) in hippocampal neurons; inset, micrograph showing
617 the setup for EPSC recordings from a hippocampal neuron (scale bar, 20 μm). (C) As
618 in (A), except that 50 μM BAPTA-AM was pre-loaded into the DRG and DH neurons
619 before recording in Ca^{2+} -free (black) or 2 mM Ca^{2+} -containing solution (green). (D)
620 Left, quantification of amplitude as in (A) ($n = 26$ cells for 0Ca^{2+} and 29 cells for
621 2Ca^{2+}). Right, quantification of EPSC amplitudes as in (C) ($n = 16$ cells for 0Ca^{2+} and
622 14 cells for 2Ca^{2+}). (E) Evoked CiVDS-EPSCs (0Ca^{2+} , black) and total EPSCs (CDS
623 + CiVDS, 2Ca^{2+} , green) induced by paired-pulse stimulation with a 50-ms interval
624 from DH neurons co-cultured with DRG neurons. The 0Ca^{2+} and 2Ca^{2+} EPSCs were
625 recorded in 2 different DH neurons. (F) Summary plot of paired-pulse ratios as in (E)
626 with different intervals (in 0Ca^{2+} , $n = 7$ cells for 10 ms, 13 for 50 ms, 14 for 500 ms,
627 10 for 5 s, and 8 for 15 s; in 2Ca^{2+} , $n = 14$ cells for 10 ms, 17 for 50 ms, 22 for 500 ms,
628 19 for 5 s, and 14 for 15 s). Inset shows the initial plot at an expanded scale. (G)
629 Representative EPSCs induced by a 10-Hz stimulus train in DH neurons co-cultured
630 with DRG neurons in Ca^{2+} -free (black) or 2 mM Ca^{2+} -containing solution (green).
631 The 0Ca^{2+} and 2Ca^{2+} EPSCs were recorded in 2 different DH neurons. (H) Summary
632 plots of the EPSC amplitudes as in (G), including CiVDS (0Ca^{2+} , black), CDS +

633 CiVDS (2Ca^{2+} , green), and CDS ($2\text{Ca}^{2+} - 0\text{Ca}^{2+}$, blue) ($n = 11$ cells). (I) As in (H),
634 statistics for amplitudes of CiVDS-EPSC (0Ca^{2+} , black) and CDS-EPSC (“ 2Ca^{2+} ” –
635 “ 0Ca^{2+} ”, blue) evoked by single-pulse (first EPSC, left) or 10 pulses (cumulative 10
636 EPSCs, Σ_{EPSC} , right) during 10-Hz train stimulation ($n = 11$ cells). All but (B) were
637 from DRG and DH co-cultures. Data are shown as the mean \pm s.e.m.; Mann-Whitney
638 test for D and F; paired Student’s t test for I; * $p < 0.05$, ** $p < 0.01$, *** $p < 0.001$, ns,
639 not significant.

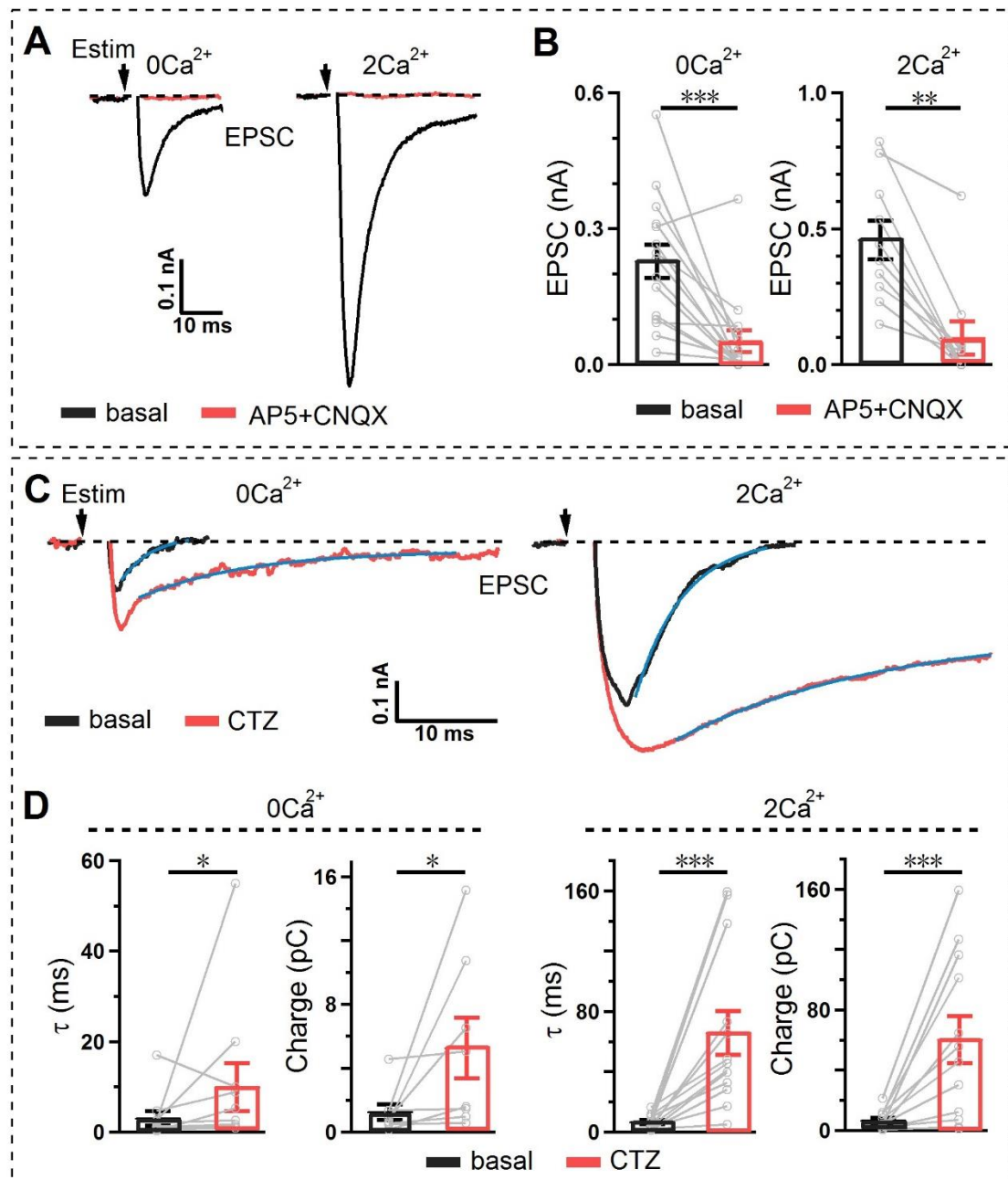
640

641



642 **Figure 2.** Imaging of CiVDS mediated synaptic transmission in co-cultured DRG and
643 DH neurons. (A) A representative photograph showing the co-cultured DRG and DH
644 neurons. The DRG neurons were expressed with Spy-pHluorin for imaging the

645 synaptic transmission. Scale bar, 10 μm . (B) Images of a presynaptic bouton marked
646 in (A) showing the Spy-pHluorin fluorescence at 20 s before (-20 s, pre-stimulus), 20
647 s, 40 s, and 120 s after electrical stimulation (post-stimulus) in 0Ca^{2+} (upper panel) or
648 2Ca^{2+} (lower panel) solution. (C) Averaged fluorescence changes ($\Delta F/F_0$) of
649 Spy-pHluorin in 0Ca^{2+} (left) or 2Ca^{2+} solution (right) in response to the same
650 electrical stimulation (20 Hz, 20 s) ($n = 45$ puncta from 6 cells for 0Ca^{2+} and 57
651 puncta from 6 cells for 2Ca^{2+}). The shadow in the traces represents the error bars
652 (s.e.m) of each point. (D-F) The same as in (A-C), but the experiments were
653 performed in cultured hippocampal neurons ($n = 70$ puncta from 3 cells for 0Ca^{2+} and
654 72 puncta from 3 cells for 2Ca^{2+}).
655



656

657 **Figure 3.** The CiVDS-EPSC is mediated by glutamate transmission. (A)

658 Representative evoked EPSCs in DH neurons co-cultured with DRG neurons before

659 (black) and after (red) applying 50 μ M AP-5 and 10 μ M CNQX in Ca^{2+} -free (left) or 2

660 mM Ca^{2+} -containing solution (right). The EPSCs of $0Ca^{2+}$ and $2Ca^{2+}$ were recorded in

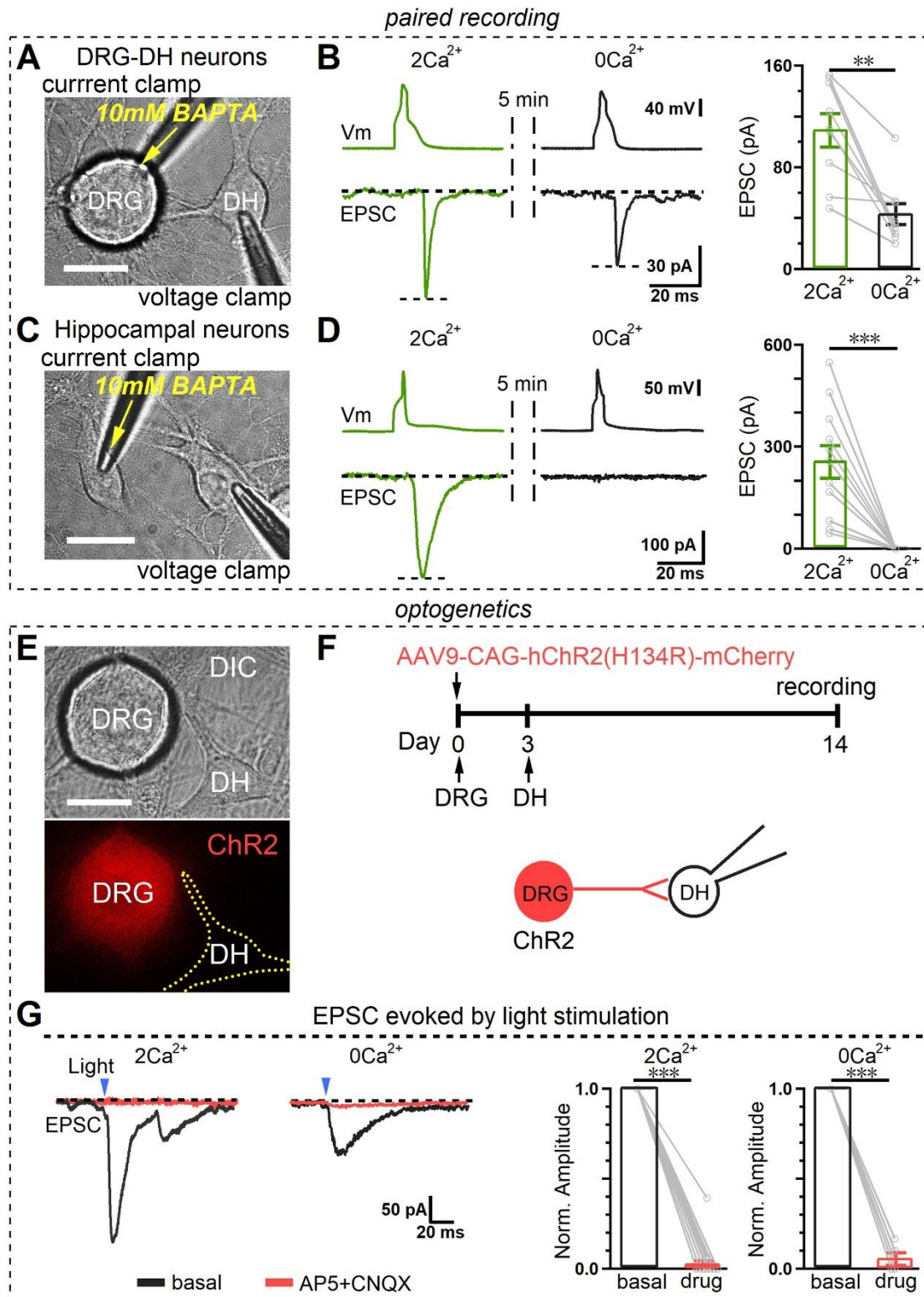
661 2 different DH neurons. (B) Quantification of EPSC amplitudes as in (A) (n = 15 cells

662 for $0Ca^{2+}$ and 10 cells for $2Ca^{2+}$). (C) Evoked EPSCs recorded in DH neurons

663 co-cultured with DRG neurons before (black) and after (red) applying 100 μM
664 cyclothiazide (CTZ) in 0Ca^{2+} (left) or 2Ca^{2+} solution (right). The traces are fitted with
665 a single exponential curve (blue). The EPSCs of 0Ca^{2+} and 2Ca^{2+} were recorded in 2
666 different DH neurons. (D) Quantification of the decay time (τ) and charge as in (C) (n
667 = 10 cells for 0Ca^{2+} and 12 cells for 2Ca^{2+}). EPSCs were evoked by local electrical
668 stimulation (Estim) at arrows. Data are shown as the mean \pm s.e.m.; paired Student's t
669 test; * $p < 0.05$, ** $p < 0.01$, *** $p < 0.001$.

670

671

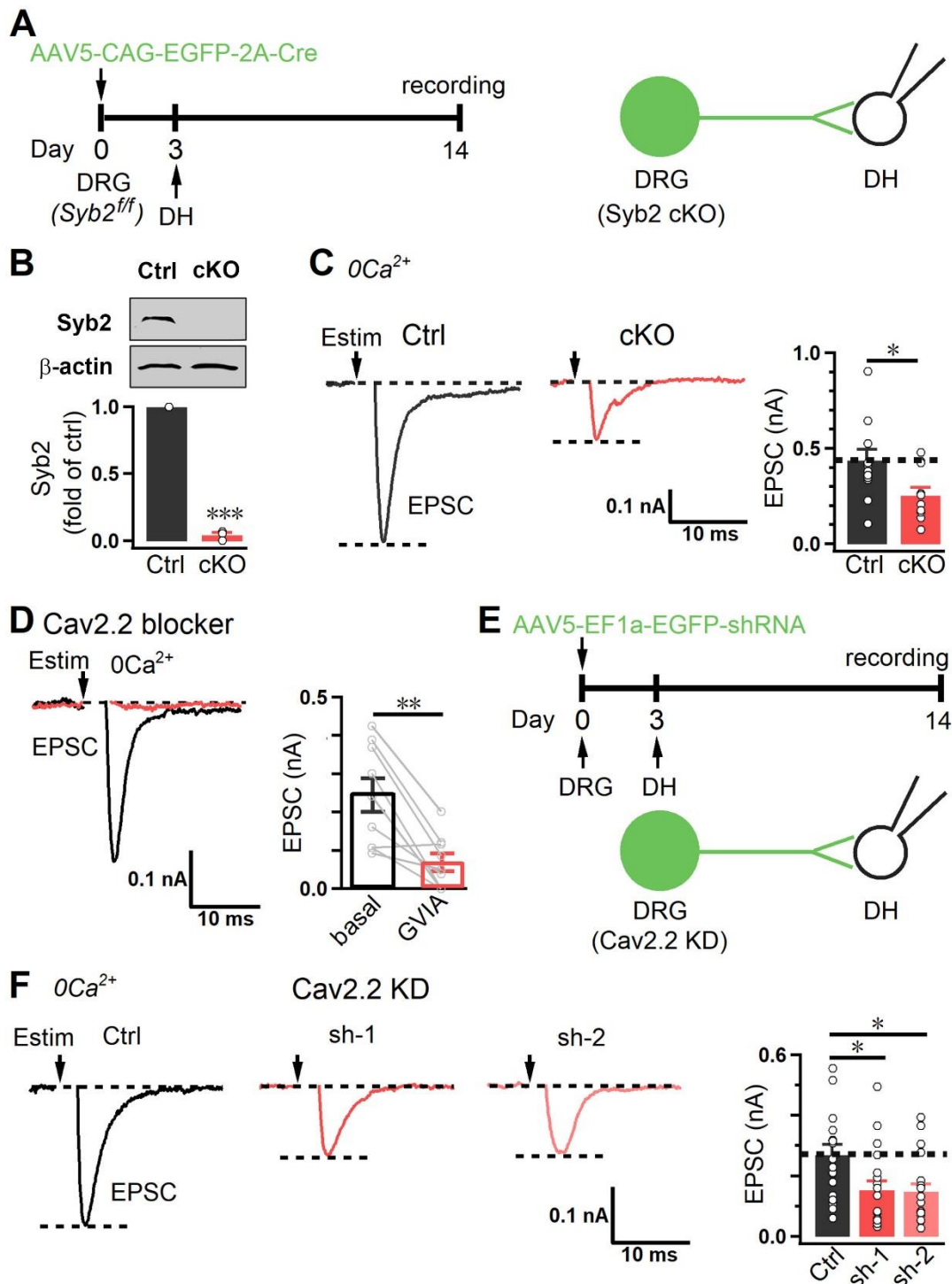


672 **Figure 4.** Presynaptic DRG neurons elicit CiVDS-EPSCs in postsynaptic DH neurons.

673 (A) Setup for paired patch-clamp recording of dorsal root ganglion (DRG) and dorsal

674 horn (DH) neurons in co-culture. The presynaptic DRG neuron was whole-cell

675 dialyzed with 10 mM BAPTA under current-clamp mode, while the postsynaptic DH
676 neuron was in voltage-clamp mode. (B) Left, representative dual recordings of
677 presynaptic action potentials (upper) and postsynaptic EPSCs (lower) following
678 current-step injection (1000 pA, 5 ms) in a DRG neuron dialyzed with 10 mM
679 BAPTA. Following whole-cell break-in and intracellular BAPTA dialysis, double
680 recordings were performed at 0 min / 2.5 mM Ca²⁺ bath (green), and 5 min / 0 Ca²⁺
681 bath (black), Right, statistics of EPSC amplitudes (n = 9 cells). (C and D) As in (A
682 and B), except that EPSCs were recorded from cultured hippocampal neurons (n = 11
683 cells). (E) Image showing a DRG neuron infected by ChR2-mCherry AAV2/9 virus
684 and a co-cultured DH neuron. (F) Upper, diagram showing the protocol for infection
685 of DRG neurons by ChR2-mCherry virus and co-culture with DH neurons; lower,
686 cartoon of EPSC recording from DH neurons co-cultured with ChR2-expressing DRG
687 neurons. (G) Left, typical EPSCs from DH neurons induced by light stimulation (475
688 nm, 5 ms, at arrows) of co-cultured ChR2-expressing DRG neurons in Ca²⁺-free or 2
689 mM Ca²⁺-containing solution before (black) and after (red) exposure to 50 μM AP5
690 and 10 μM CNQX. The EPSCs of 0Ca²⁺ and 2Ca²⁺ were recorded in 2 different DH
691 neurons; right, statistics of EPSC amplitude (n = 5 cells for 0Ca²⁺ and 14 for 2Ca²⁺).
692 Data are shown as the mean ± s.e.m.; Wilcoxon test for B; paired Student's *t* test for D
693 and G; **p <0.01, ***p <0.001. Scale bars, 20 μm.
694



695

696 **Figure 5.** CiVDS-EPSCs are mediated by the SNARE complex and N-type

697 Ca²⁺-channels. (A) Left, diagram showing the protocol for EPSC recording from DH

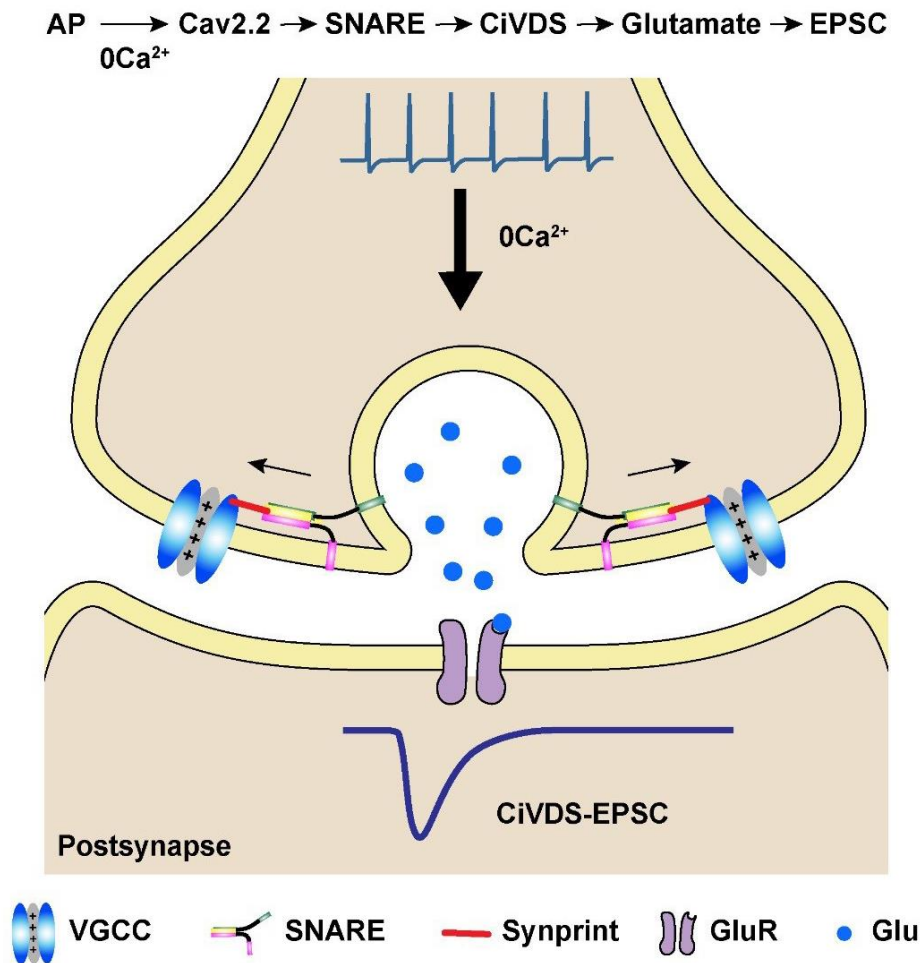
698 neurons co-cultured with Syb2-knockout (cKO) DRG neurons; right, cartoon of EPSC

699 recording from DH neurons co-cultured with Syb2-cKO DRG neurons. (B)

700 Representative western blots (upper) and analysis (lower) of the expression levels of
701 Syb2 in control (Ctrl) and Syb2-cKO DRG neurons (n = 3 per group). (C) Evoked
702 EPSCs and statistics from DH neurons co-cultured with control (Ctrl) or Syb2-cKO
703 DRG cells (cKO) in 0Ca^{2+} solution (n = 13 cells for Ctrl and 11 for cKO). (D) Evoked
704 EPSCs and statistics from DH neurons co-cultured with DRG neurons before (black)
705 and after (red) applying $1\ \mu\text{M}$ ω -conotoxin-GVIA (GVIA) in 0Ca^{2+} bath (n = 9 cells).
706 (E) Upper, diagram showing the protocol for EPSC recordings from DH neurons
707 co-cultured with Cav2.2 knockdown (KD) DRG neurons; lower, cartoon of EPSC
708 recording from DH neurons co-cultured with Cav2.2-KD DRG neurons. (F) Left
709 panels, evoked EPSCs from DH neurons co-cultured with control (Ctrl) or Cav2.2-KD
710 (sh-1/sh-2) DRG neurons in 0Ca^{2+} solution. Right panel, quantification of evoked
711 EPSCs (n = 17 cells for Ctrl, 12 for sh-1, and 19 for sh-2). EPSCs were evoked by
712 local electrical stimulation (Estim, at arrows). Data are shown as the mean \pm s.e.m.;
713 paired Student's *t* test for B and D, unpaired Student's *t* test for C, and Kruskal-Wallis
714 test followed by Dunn's multiple comparisons test for F; *p <0.05, **p <0.01, ***p
715 <0.001.

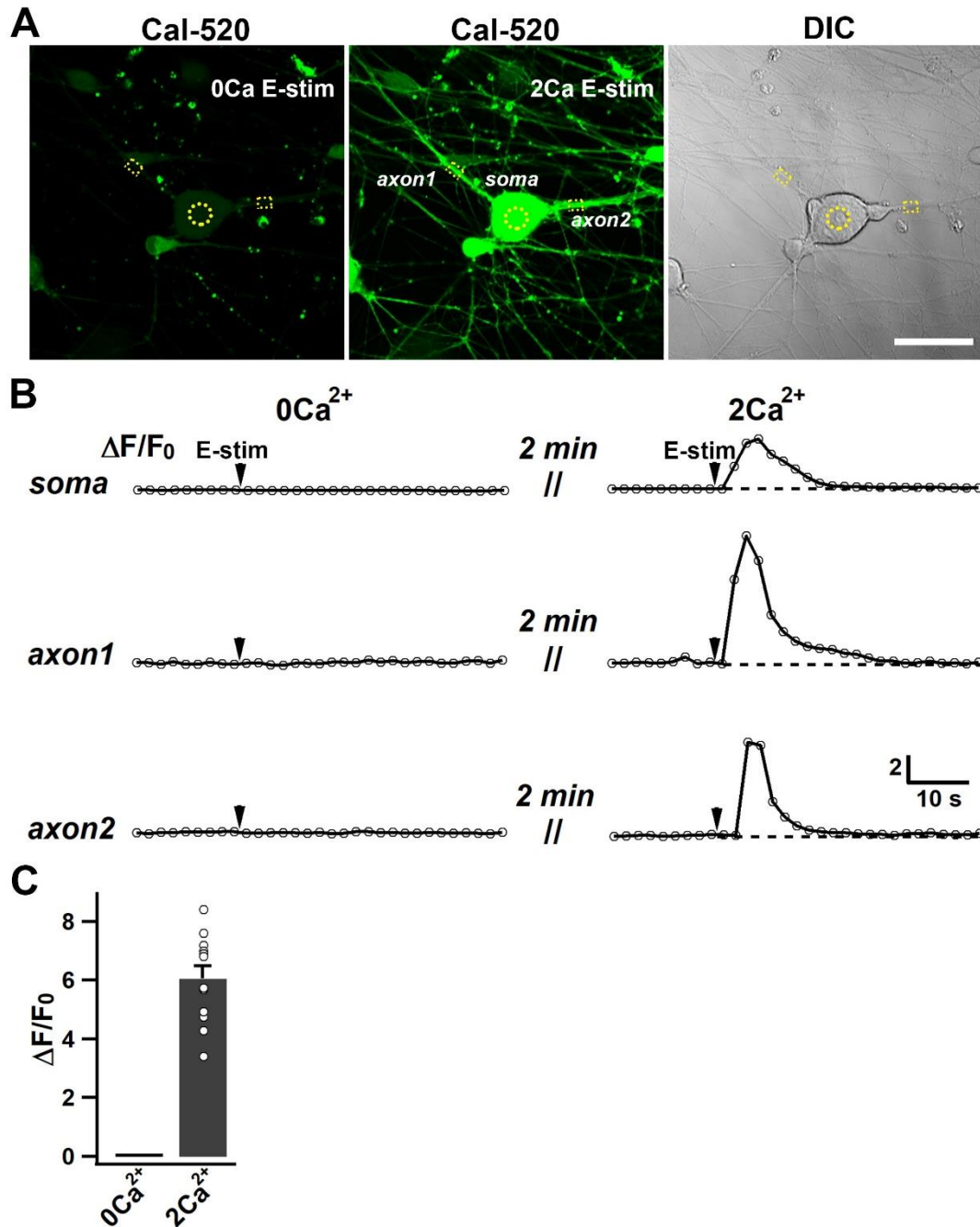
716

717



718 **Figure 6.** A model of the CiVDS-mediated EPSC in synaptic transmission. In
719 Ca^{2+} -free bath, an action potential activates the voltage-gated Ca^{2+} channel
720 (VGCC/Cav2.2) and triggers presynaptic glutamate release through Ca^{2+} -independent
721 but voltage-dependent secretion (CiVDS), and activates an excitatory postsynaptic
722 current (CiVDS-EPSC). In physiological solution containing Ca^{2+} , however, both
723 CiVDS- and Ca^{2+} -dependent secretion (CDS)-mediated glutamate release contribute
724 to a larger evoked postsynaptic EPSC (not shown).

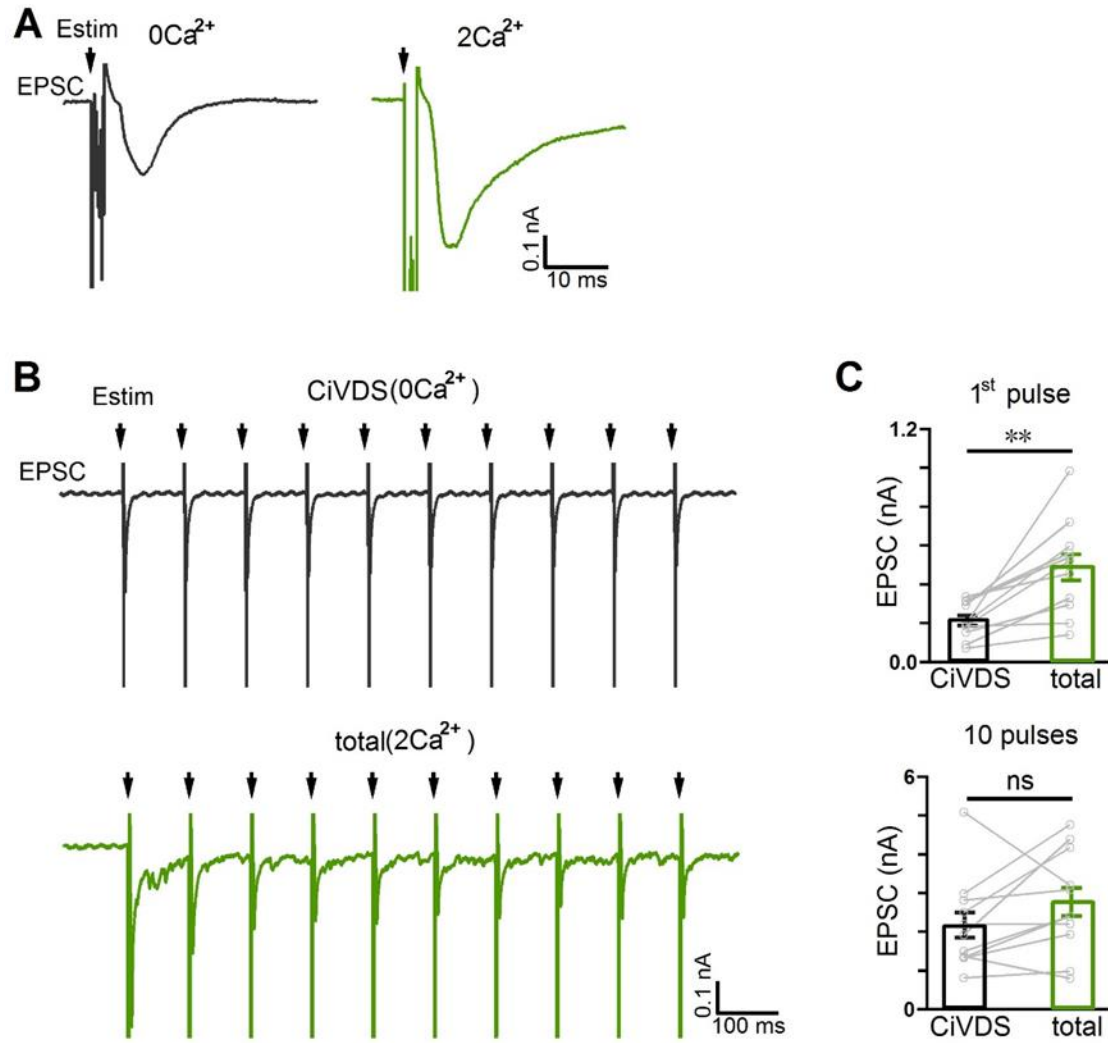
725



726

727 **Figure 1—figure supplement 1.** Absence of intracellular Ca²⁺ signal ($\Delta F/F_0$) in DRG
728 neurons in Ca²⁺-free solution. (A) Representative images showing the loading of
729 Cal-520 in co-cultured DRG and DH neurons (scale bar, 50 μ m; DIC, differential
730 interference contrast). (B) Ca²⁺ signal $\Delta F/F_0$ of Cal-520 fluorescence induced by

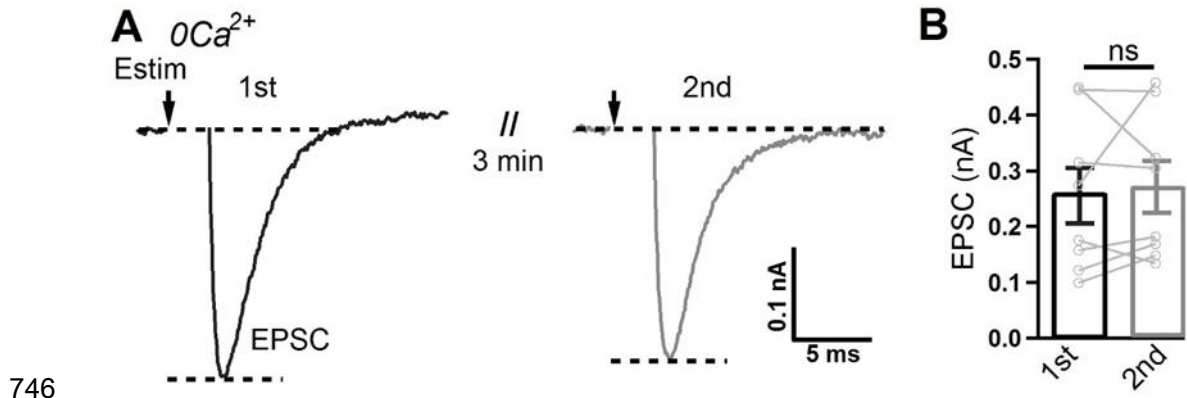
731 electrical stimulation (E-stim at arrows) in Ca^{2+} -free (left) and 2 mM Ca^{2+} -containing
732 solution (right) from typical regions labeled in (A). (C) Statistics of $[\text{Ca}^{2+}]_i$ rise as in
733 (B) ($n = 12$ cells). No $[\text{Ca}^{2+}]_i$ rise in Ca^{2+} -free solution was detectable. Data are shown
734 as the mean \pm s.e.m. Student's t test for (C); *** $p < 0.001$.



735

736 **Figure 1—figure supplement 2.** EPSCs evoked by local-field electrical stimuli from
737 DH neurons co-cultured with DRG neurons. (A) Original recordings of EPSCs
738 including artifacts in response to a single electrical stimulus (Estim, arrows) in $0Ca^{2+}$
739 ($0Ca^{2+}$ and $2Ca^{2+}$ were recorded in different DH neurons. (B) As in (A) for CiVDS ($0Ca^{2+}$) or total (CiVDS
740 +CDS, $2Ca^{2+}$), but in response to a 10-Hz train of 10 pulses. The EPSCs of $0Ca^{2+}$ and
741 $2Ca^{2+}$ were recorded in different DH neurons. (C) Statistics of CiVDS-EPSC ($0Ca^{2+}$,
742 black) and total (CDS + CiVDS)-EPSC ($2Ca^{2+}$, green) evoked by single (first) pulse
743 or 10 pulses during 10-Hz train stimulation as in (B) (n = 11 cells). Data are shown as
744

745 mean \pm s.e.m.; paired Student's *t* test for (C), ***p* < 0.01, ns, not significant.



746

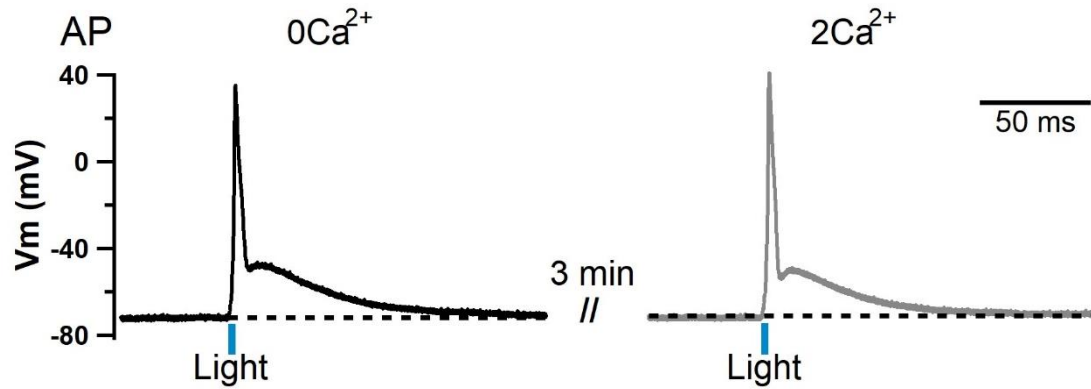
747 **Figure 3—figure supplement 1.** CiVDS-EPSC is reproducible during a repeated

748 stimulus. (A) CiVDS-EPSCs induced by electrical stimulation (Estim, arrows)

749 repeated after a 3-min interval in a DH neuron co-cultured with DRG neurons in

750 $0Ca^{2+}$ solution. (B) Quantification of EPSC amplitude as in (A) ($n = 8$ cells). Data are

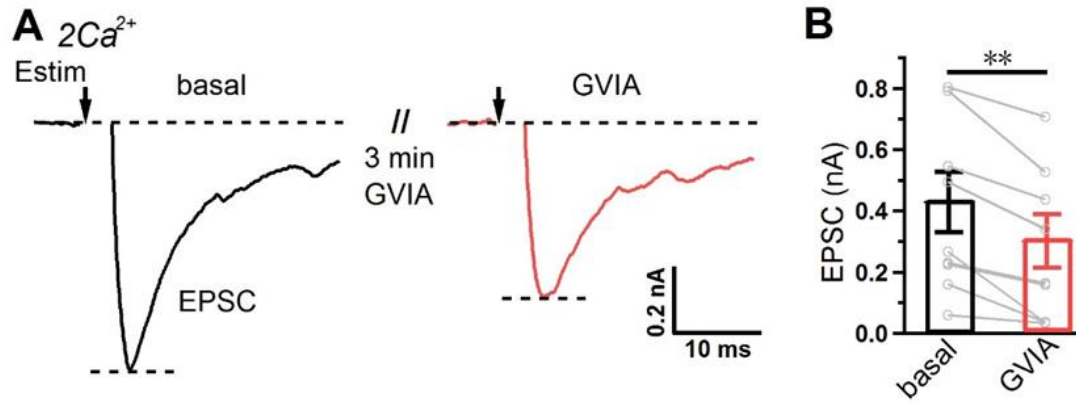
751 shown as the mean \pm s.e.m.; paired Student's t test for (B); ns, not significant.



752

753 **Figure 4—figure supplement 1.** Light-evoked action potentials in DRG neurons
754 expressing ChR2. Representative action potentials (APs) evoked by light stimulation
755 (475 nm, 5 ms) in a ChR2-expressing DRG neuron in 0Ca^{2+} (left) and 2Ca^{2+} (right)
756 solutions.

757



758

759 **Figure 5—figure supplement 1.** EPSCs in DH neurons co-cultured with DRG

760 neurons are partially blocked by the Cav2.2 inhibitor GVIA. (A) EPSCs induced by

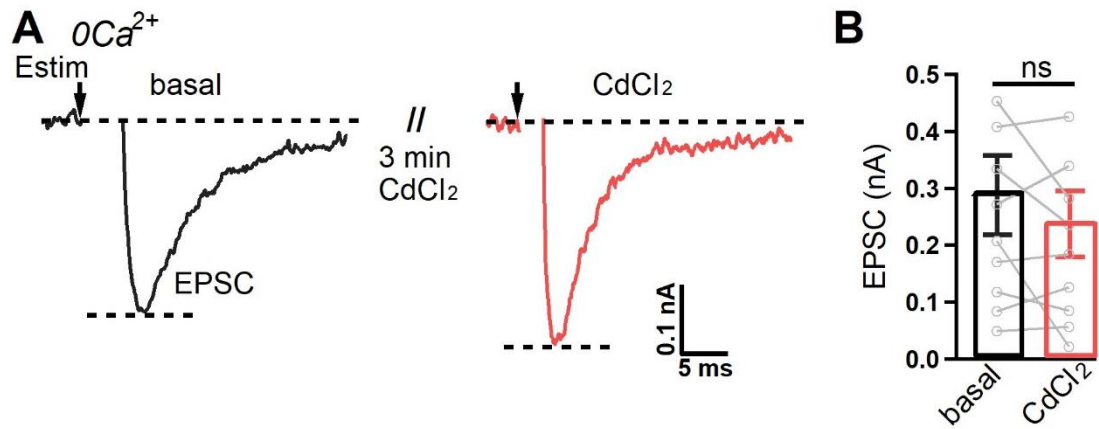
761 electrical stimulation (Estim, at arrows) in a DH neuron co-cultured with DRG

762 neurons before (black) and after (red) 1 μ M ω -conotoxin-GVIA (GVIA) application in

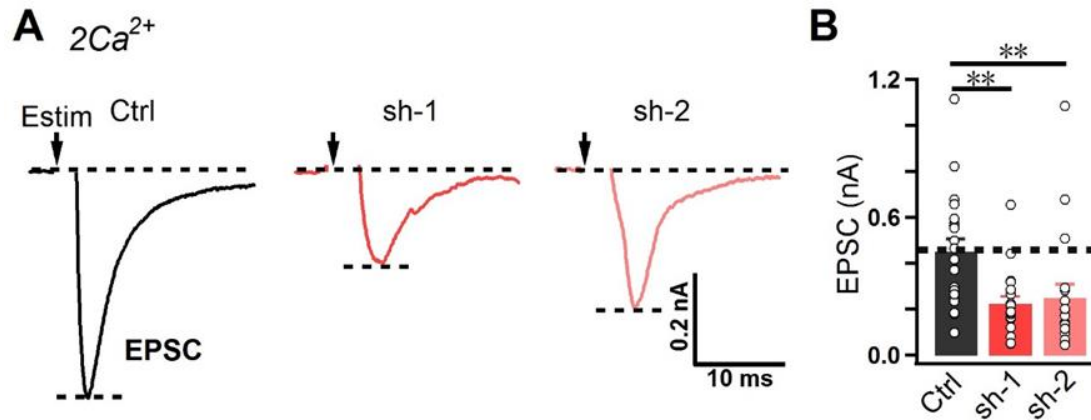
763 $2Ca^{2+}$ solution. (B) Quantification of EPSC amplitudes as in (A) (n = 9 cells). Data

764 are shown as the mean \pm s.e.m.; paired Student's *t* test for (B); ***p* < 0.01.

765



766 **Figure 5—figure supplement 2.** CiVDS-EPSCs in DH neurons co-cultured with
767 DRG neurons are insensitive to CdCl₂. (A) EPSCs induced by electrical stimulation
768 (Estim, arrows) in a DH neuron co-cultured with DRG neurons before (basal) and
769 after 100 μ M CdCl₂ application (CdCl₂) in $0Ca^{2+}$ solution. (B) Quantification of
770 EPSC amplitudes as in (A) (n = 10 cells). Data are shown as the mean \pm s.e.m.; paired
771 Student's *t* test for (B); ns, not significant.
772



773

774 **Figure 5—figure supplement 3.** EPSCs in DH neurons co-cultured with DRG

775 neurons are partially blocked by Cav2.2 knockdown. (A) Typical EPSCs induced by

776 electrical stimulation (Estim, arrows) in DH neurons co-cultured with control (Ctrl) or

777 Cav2.2-KD virus (sh-1/sh-2)-infected DRG neurons in 2 mM Ca^{2+} -containing

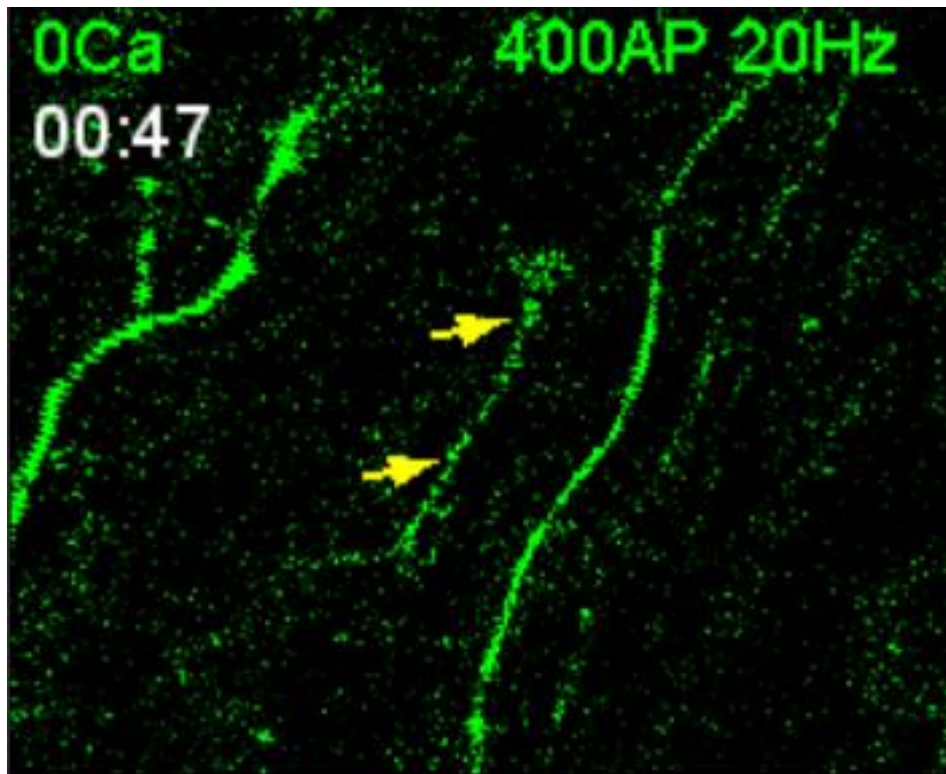
778 solution. (B) Quantification of EPSC amplitude as in (A) (n = 18 cells for Ctrl, 15 for

779 sh-1, and 19 for sh-2). Data are shown as the mean \pm s.e.m.; Kruskal-Wallis test

780 followed by Dunn's multiple comparisons test for (B); **p < 0.01.

781

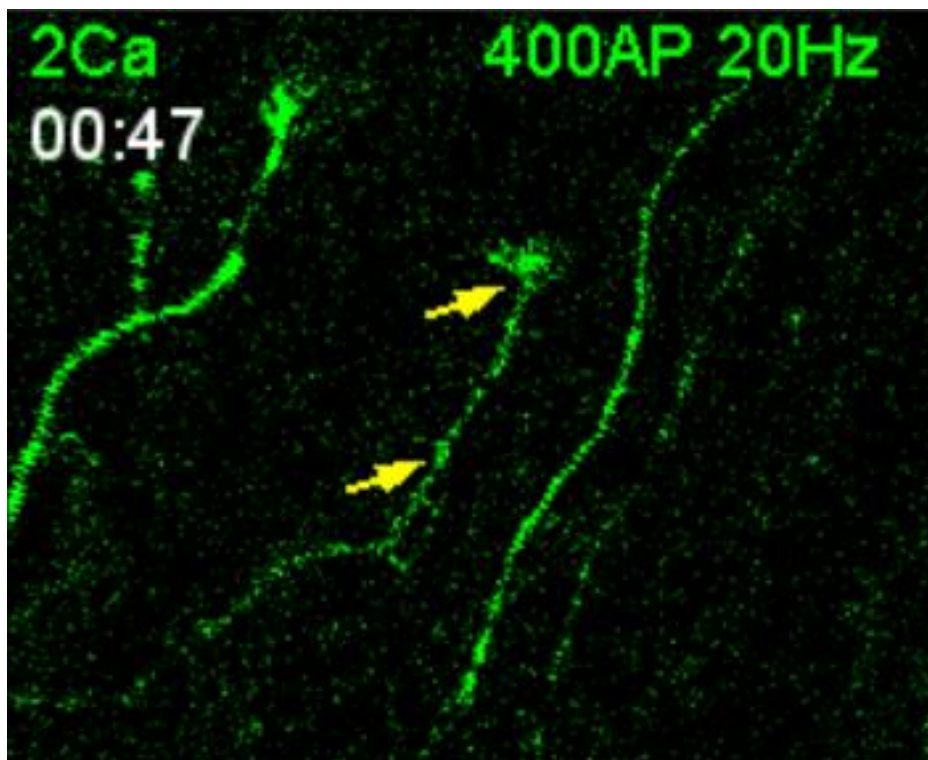
782



783

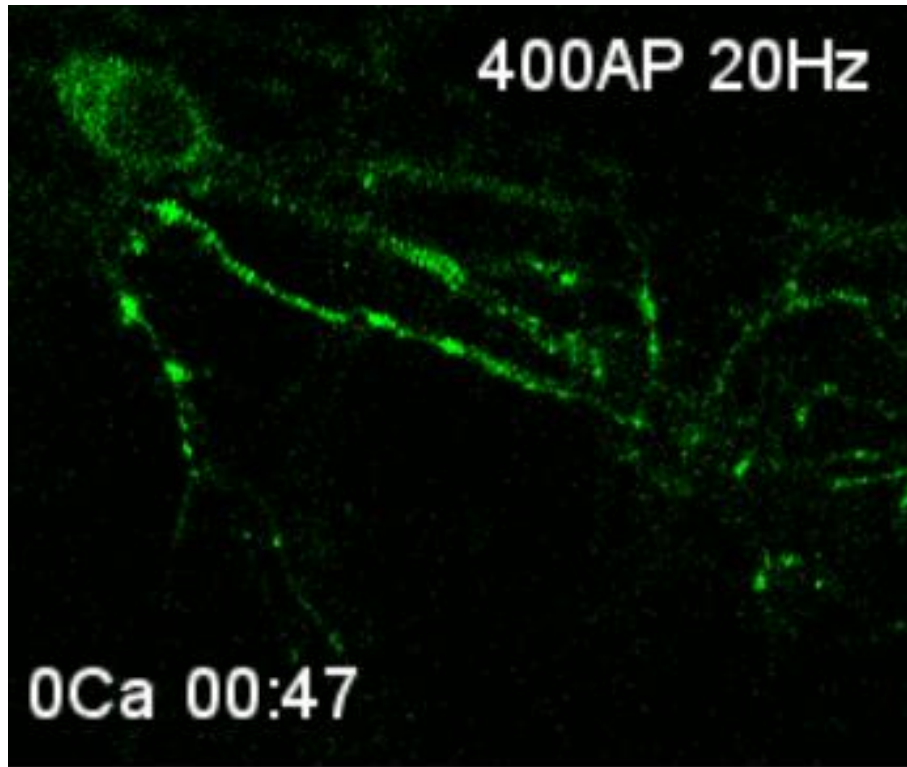
784 **Figure 2-video 1. Spy-pHluorin signal from DRG-DH neuron in 0Ca solution.**

785



786

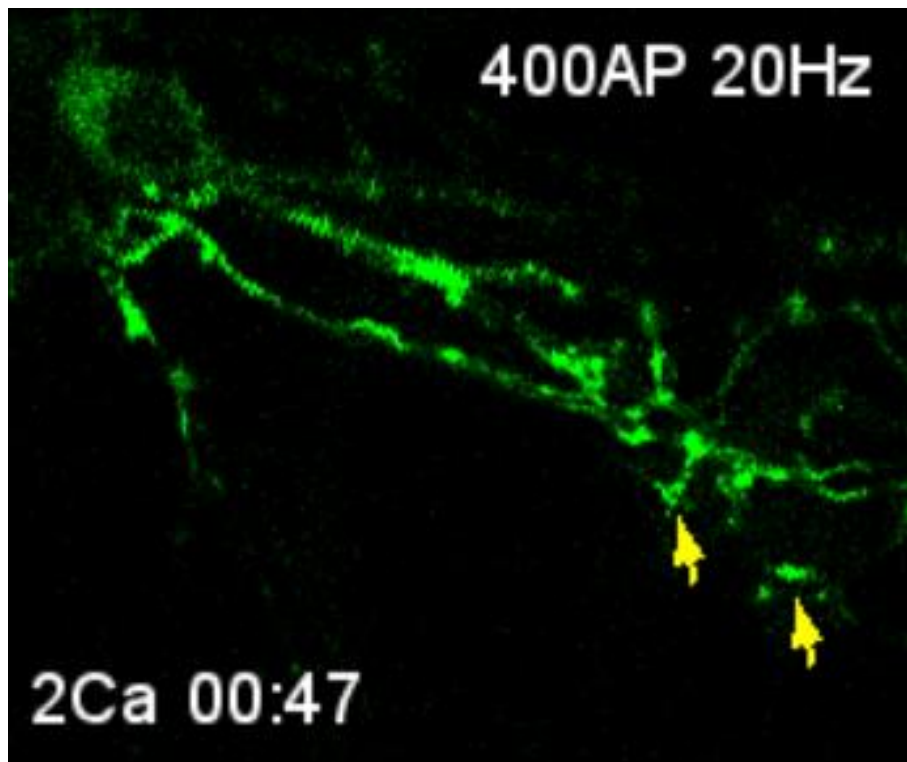
787 **Figure 2-video 2. Spy-pHluorin signal from DRG-DH neuron in 2Ca solution.**



788

789 **Figure 2-video 3. Spy-pHluorin signal from hippocampal neuron in 0Ca solution.**

790



791

792 **Figure 2-video 4. Spy-pHluorin signal from hippocampal neuron in 2Ca solution.**